Integrated Fibre Cavity for Quantum Networks

Pia Johanna Fürtjes

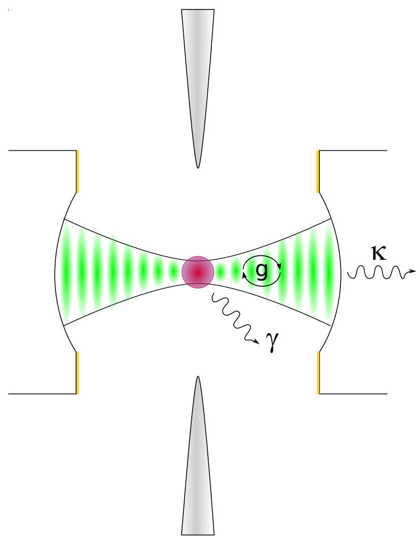

Masterarbeit in Physik
angefertigt im Physikalischen Institut

vorgelegt der
Mathematisch-Naturwissenschaftlichen Fakultät
der
Rheinischen Friedrich-Wilhelms-Universität
Bonn

Oktober 2018

I hereby declare that this thesis was formulated by myself and that no sources or tools other than those cited were used.

Bonn, ...

Date Signature

1. Gutachter: Prof. Dr. Michael Köhl
2. Gutachter: Prof. Dr. Dieter Meschede

Acknowledgements

Firstly, I would like to thank Prof. Michael Köhl for giving me the opportunity of writing my master thesis in his research group. Thanks for reviewing the project and to adapt and extend it from time to time to make it a feasible work during this year.

I would also like to thank Dr. Hendrik Meyer for supervising me in the first half year of the project, for all his knowledge who helped me building, designing and understanding the work in the lab and for proofreading this thesis. Thanks to Thorsten Langerfeld for the technical and human support, for the discussions and the great collaboration.

I would also like to thank Prof. Dieter Meschede for the friendly cooperation, for providing the facilities where this work has been build up and for being the second referee. Thanks to Michael Kubista for nicely introducing me into the former setup, to Deepak Pandey and Wolfgang Alt for all discussions during our weekly meetings and the sharing of knowledge and experience. Thanks to David Röser for being a comfortable lab companion and for the cooperation when setting the elements who required more than two hands. Also, I would like to thank Prof. Stefan Linden and Alexander Fassbender for the cooperation and the effort of writing structure on the desired end facets.

A special thanks goes to the entire group, especially Marcell and Thorsten for all the laughs who encouraged me in the unpleasant moments. It is good to have so many people around which are happy to help you with any problems. It was a pleasure to spend one year with you! Thanks to Nicola for proofreading this thesis.
Thanks to Anne Schnell for all the support concerning chemical questions and for soaking the fibres in multiple acids, I should not have done on my own!

Also I would like to thank Walther Ockenfels for trying his best to attach wire bonds onto the gold coating and the mechanical workshop of the *Physikalisches Institut der Universität Bonn* for the great effort of producing many fibre holders. For financial support, I would like to thank the SFB/TR 185 Project A2.

Contents

1 Introduction **7**

2 Resonators and Light-Matter Interactions **11**
- 2.1 Optical Resonators . . . 11
  - 2.1.1 Fabry-Perot Resonator . . . 11
  - 2.1.2 Fibre Cavity . . . 13
- 2.2 Atom-Light Interaction . . . 15
- 2.3 Ion traps with integrated cavity . . . 17

3 Fibre End Facet Machining **19**
- 3.1 Setup Elements . . . 20
- 3.2 Machining Elements . . . 23
- 3.3 Results . . . 31
  - 3.3.1 Criteria for Mirror Geometries . . . 31
  - 3.3.2 Cleaving Fibres . . . 31
  - 3.3.3 Pulse Sequence . . . 33
  - 3.3.4 Analysis of Obtained Structures . . . 35

4 Towards Integrated Electrodes on Fibre Mirrors **41**
- 4.1 Paul Traps . . . 41
- 4.2 Motivation . . . 43
- 4.3 Realisation . . . 44

5 Conclusion and Outlook **49**

A Appendix **51**
- A.1 General Notes and Remarks . . . 51
- A.2 Gaussian Beams . . . 52

Bibliography **53**

CHAPTER 1

Introduction

With the growing understanding and the ability of manipulating quantum systems, Kimble suggested in 2008 the realisation of a quantum internet [1] comprising quantum nodes and quantum channels which would allow to distribute quantum information. As a classical computer, stationary qubits interacting with each other are required for building gates for quantum computing. In a quantum node, the quantum information is generated, processed and locally stored and linked via a quantum channel to other quantum nodes. This quantum channel transports the information about the quantum state from one site to another. The information storage is done in so called stationary qubits and the information is transferred using flying qubits which can be distributed over the network. In a quantum node, the stationary qubits are interacting with flying qubits via a strong interface and perform quantum state transfer. The scientific community is currently exploring systems of single quantum states in the field of quantum dots [2], single ions [3], neutral atoms [4] and nitrogen-vacancy centres [5]. The technological development is challenging and requires new techniques in order to built apparatuses which can efficiently handle systems of such small sizes.

A quantum bit is the quantum mechanical equivalent to a classical bit. A classical bit can represent the numerical bits 0 and 1 and can store the information in the binary system. The quantum bit can be in the eigenstate $|0\rangle$ and $|1\rangle$ and undergo a superposition of these two states. In general, a quantum mechanical bit can be written as $|\Psi\rangle = \alpha\,|0\rangle + \beta\,|1\rangle$, where α and β are complex numbers. The fact that a quantum state can represent a superposition of two eigenstates challenges numerical problems of classical computation, i.e. allowing to accomplish prime factorisation used in public key encryption in a reasonable amount of time [6]. In the experiment, a quantum bit is represented by two mechanically distinguishable internal quantum states in one quantum system having a closed transition and interacting via an interface with each other.

Ions in Paul traps are promising candidates for the implementation of stationary quantum bits [7]. A quantum bit state is a specific electronic configuration of the internal state of an ion. Ion traps have several advantageous attributes compared to other quantum systems which make them favourable for the implementation in quantum networks. The traps can be made sufficiently deep, about 1 eV, and allow for robust trapping of single ions at room temperature despite disturbing surrounding as well as background collisions. The trapping potential does not depend on the internal electronic state of the ion and the Coulomb repulsion leads to a strong long-range interaction with other ions. It offers the opportunity to implement local gates between neighbouring ions, which themselves can have different functions. For example, it is possible to use one ion for quantum storage and one for manipulation. Lastly, the electric dipole moment of the ions leads to a strong interaction with a resonant laser field which is required for state manipulation and readout. Researchers have found a number of suitable elements whose internal electronic configuration is convenient for ion trapping in quantum networks. ^{171}Yb, for instance, has a very advantageous electronic ground state appropriate for quantum operations and is used preferably in recent experiments [8].

In order to perform quantum operations on ions, the internal electronic state configuration must be accessible with available lasers, i.e. the laser's wavelength needs to correspond to a specific energy difference that matches the energy difference between two state levels. In addition, the ions must provide a stable ground state and a long lived excited state for the qubit states $|0\rangle$ and $|1\rangle$, as well as a short lived excited state needed for cooling processes. The transition between the states $|0\rangle$ and $|1\rangle$ must be a closed transition to ensure proper manipulation and readout of the qubit. A Paul trap is a specific ion trap type that uses alternating electric fields to create a local minimum in the quadrupole center. The trapping of ions is generally only possible if the trap depth exceeds the kinetic energy of the ion. Keeping the kinetic energy low and cooling the ion for maintaining a good trap stability is done via photon absorption and emission which requires the aforementioned short lived excited state. There are several Paul trap configurations which allow for single and multiple ion trapping depending on the electrode configuration.

As soon as one has the ability of trapping, a reliable manipulation of the electronic ion state is needed. An efficient optical interface which enables strong coupling between a resonant light field and the ion ensures that the absorption and emission of single photons inside the resonator becomes a reversible process. Also, strong coupling leads to an enhanced photon emission into the cavity mode which is essential for state readout. This system allows for studying fundamental and simple atom-photon interactions, such as of the Purcell effect [9]. One approach for creating optical interfaces is the construction of an optical resonator around the trap center where the ion is located. Such a resonator, also called cavity, consists of two mirrors facing each other which stores a light field due to multiple back and forth reflections and favours the absorption as well as the extraction and emission process of a photon. The progress moves towards miniaturisation where physicist have found fibre cavities advantageous. The main reason for this tendency is due to the fact that the coupling between the atom and the light field is proportional to the invert square root of the mode volume. Low mode volumes are achievable with short cavities requiring mirrors of small radii of curvature. Additionally, the losses inside a resonator are inversely proportional to the finesse and the length of the cavity. Hence, mirrors of reasonably small radii of curvature are required for good performance.
The storage of a light field inside a resonator can be quantified with the finesse which

is a measure of the reflectivity and the losses of the system. In order to integrate the resonator into the trap setup, the mirror diameter shall be small enough to fit between the existing electrode structures and to leave a large optical access for coherent manipulation and readout. As the light field exiting the resonator travels inside the fibres, the connection to existing networks is easy since no further optics are required to link multiple photonic interfaces. Macroscopic mirrors require much more space and do not fit at the desired length into the setup. Working in vacuum minimizes any disturbing effects on the ion and is the reason why the resonator cannot be implemented within a glass substrate with anti-reflection coating. Even though the alignment is much more difficult, a resonator consisting of two individual mirrors is adjustable in length and is therefore tunable for different wavelengths.

If one aims for cavities of a length of a few hundred micrometers, the mirror sphere radii need to be of the same order of magnitude for building stable resonators. A spheric shape with a well chosen curvature is fabricated onto a fibre end facets and combined with a high reflectance coating which creates a miniaturised mirror. The fabrication of such fibre mirrors is a very subtle task and requires a precise setup with a well-controllable laser beam of infrared light. Shaping fibre end facets is possible with a CO_2 laser which runs at a wavelength of 9.3 µm and is focussed to small waist sizes. Glass is highly absorptive for this wavelength and ablation processes deform the surface and create spherical structures in the micrometer regime. High-reflection and anti-reflection coatings consisting of multiple layers of dielectric materials are evaporated to a certain thickness onto the fibre surface to create a mirror. The coating quality and the surface shape is decisive for the finesse of a fibre cavity.

However, in the case of ion traps, dielectric surfaces have a negative effect on the trapping performance as the mirrors are brought close to the ion and stray charges accumulate on the surface which severely disturb the trapping performance. The stray fields prohibit to built a quantum gate inside an ion trap due to limited cooling abilities. An ion is only a good stationary qubit if it has a stable ground state which cooled below the sub-Doppler limit which is not possible with the current fibre mirrors. In effort to counteract the limited cooling, another additional conductive layer is coated onto the fibre mirrors to minimize the effect of stray fields. Overall, this work aims for the experimental implementation of a quantum node in ion traps which requires the improvement of optical interfaces.

CHAPTER 2

Resonators and Light-Matter Interactions

The ability of constructing cavities and ion traps has been evolving over the last decades and did contribute to the knowledge of cavity quantum electrodynamics [8, 10]. The progress leading toward miniaturisation of experimental components is the base for studying quantum systems in its simplest form. The physics of atom-photon interaction becomes interesting when the atom is placed inside a high finesse resonator. This chapter introduces the physics of optical resonators and outlines under which conditions light-matter interaction can be studied.

2.1 Optical Resonators

An optical resonator enhances a light field between two reflective mirror surfaces depending on the reflectivity and the losses of the mirrors, as well as on the medium inside the resonator. The following section introduces definitions and fundamental equations [11] necessary to investigate the properties of an optical resonator.

2.1.1 Fabry-Perot Resonator

Two mirror surfaces facing each other can store a light field by multiple back and forth reflections inside the resonator. The round-trip time for a single photon is given by the relation

$$t_{rt} = \frac{2L}{c}, \tag{2.1.1}$$

where L denotes the spacing between the two mirror surfaces, i.e. the cavity length, and c the speed of light. Consequently, one can define the free spectral range (FSR) as the inverse of this round-trip time, equivalent to the frequency spacing between two adjacent resonator modes

$$\omega_{\mathrm{FSR}} = 2\pi\nu_{\mathrm{FSR}} = \frac{\pi c}{L}. \tag{2.1.2}$$

Under the assumption that the resonator is lossless, the cavity finesse which describes the quality of the resonator is defined as [11]

$$\mathcal{F} = \frac{\pi\sqrt{|r_1 r_2|}}{1 - |r_1 r_2|} = \frac{\pi\sqrt[4]{\mathcal{R}_1\mathcal{R}_2}}{1 - \sqrt{\mathcal{R}_1\mathcal{R}_2}}, \tag{2.1.3}$$

r being the amplitude reflectivity and $\mathcal{R}$ the intensity reflectivity. The power fraction lost after one round-trip is given by the transmission rate $\mathcal{T} = 1 - \mathcal{R}$. The transmission spectrum of a Fabry-Perot resonator is a function of frequency and shows resonances for specific wavelengths, see figure 2.1.1. The resonance condition describes the wavelengths that have maximum transmission for a resonator of a specific length. In vacuum, it requires $n \cdot {}^{\lambda}\!/_{2} = L$, where $n \in \mathbb{N}$ in order to have a phase shift of multiples of 2π after each round-trip which constructively interfere for maximum transmission. Destructive and constructive interference of the waves inside the resonator lead to a transmission spectrum of the form

$$\mathcal{T}(\nu) = \frac{\mathcal{T}_{max}}{1 + (2\mathcal{F}/\pi)^2 \sin^2(\pi\nu/\nu_F)}. \tag{2.1.4}$$

The larger the finesse, the narrower the spectral width of the resonator modes.
The finesse of a resonator is however not only dependent on the reflectivity of the mirrors, but also is affected by losses in the system. Scattering losses $\mathcal{S}$ and absorption losses $\mathcal{A}$ negatively contribute to the width of the resonator modes. For power conservation reasons, the transmission of a cavity is given by

$$\mathcal{T} = 1 - \mathcal{R} - \mathcal{S} - \mathcal{A}. \tag{2.1.5}$$

A finesse measurement therefore detects any inaccuracies in the resonator and measures the quality of the employed mirrors.

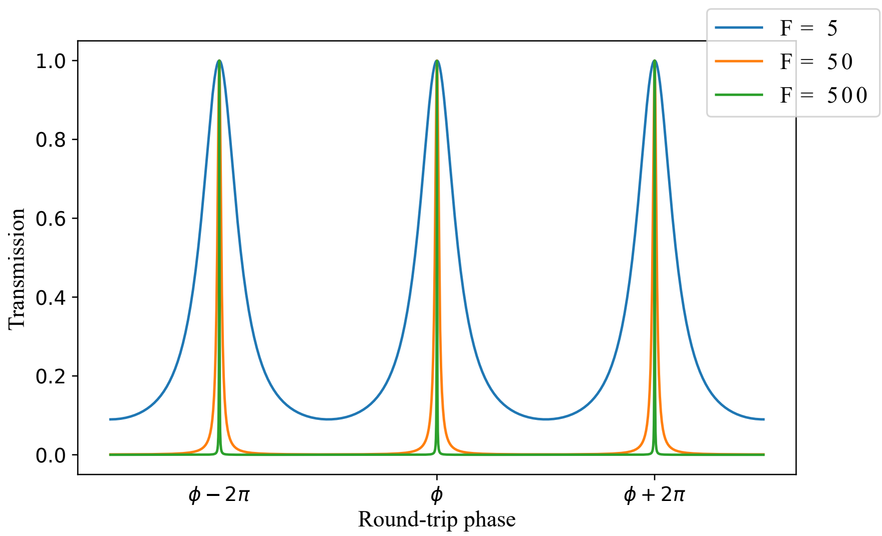

Figure 2.1.1: Transmission spectrum of a lossless cavity for different finesse values.

Accordingly, the linewidth of a resonator is given by the ratio of free spectral range and the finesse

$$\delta\omega = \frac{\omega_{\mathrm{FSR}}}{\mathcal{F}}. \tag{2.1.6}$$

An optical resonator with two arbitrarily curved mirror surfaces, see fig. 2.1.2, can either be stable or unstable. A stable cavity allows for infinite many back and forth reflections of a light field under the assumption of non-existing losses. In the case of unstable cavities, the resonator does not provide a closed circuit and the light field is reflected towards the outside of the resonator for every reflection. The determinant of a stable resonator's round-trip matrix generated from the ABCD optical formalism [11] equals unity. This is equivalent to the statement that

$$0 \leq g_1 g_2 \leq 1 \quad \text{with} \quad g_i = 1 + \frac{L}{R_i} \tag{2.1.7}$$

where R_i is the radius of curvature of a mirror surface i and is defined negative for concave mirrors (opposite convention compared to lenses). The resonator condition for two concave mirrors can further be simplified to $L \leq R_1 + R_2$ which is the relevant stability criterion for resonators [12].

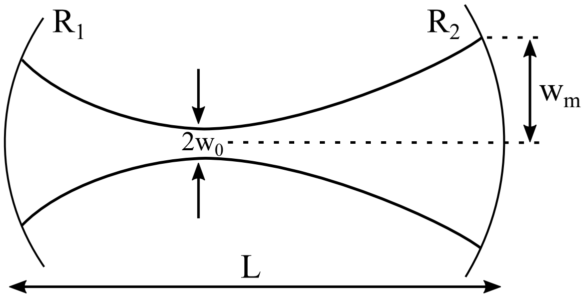

Figure 2.1.2: Geometry of an asymmetric spherical mirror resonator.

For all further investigations, it is assumed that the transversal mode profile is only given by the Gaussian ground mode and both mirror surfaces are concave. The transmission spectrum for a superposition of high order modes in the resonator has multiple peaks due to the Gouy phase of the transversal modes. For all reasonable applications, one aims only for the ground mode inside the resonator. The position and size of the minimal mode waist w_0 depends on the distance between the two mirror surfaces, their curvature and the wavelength of the light field. The same does apply to the mode waist on the mirror surfaces w_m. Their values are obtained by equalising the wavefront curvature of the Gaussian beam $R(z)$, see equation A.2.5, and the radius of curvature at the corresponding mirror R_i. Please note that z describes the spacing between w_0 and w_m, and $L = 2z$ for a symmetric cavity. Consequently, the mode waist on the mirror for a symmetric cavity is given by

$$w_m = \sqrt{\frac{\lambda R L}{\pi}} \sqrt{\frac{1}{\sqrt{2RL - L^2}}}. \tag{2.1.8}$$

The mode waist is decisive when designing the resonator geometry, including the radius of curvature and the mirror diameter.

2.1.2 Fibre Cavity

Fibre cavities are microscopic Fabry-Perot optical resonators. In this specific case, a fibre cavity is built from two optical fibres with a cladding diameter of 125 µm which can generally be adjusted to available fibre sizes. A fibre mirror is a cleaved fibre end facet with a spherical central profile and a high reflectance coating. This allows for the construction of very small resonators, nicely fitting into existing ion traps and leaving large optical access for manipulation and read out. The radius of curvature usually takes values between 150 and 300 µm and cavity lengths of typically (200 ± 50) µm for the specific case of ion traps. For other applications it might be useful to built even shorter cavities which require smaller radii of curvature, see [13]. Due to the machining technique of fibre mirrors, see chapter 3, it is possible to fabricate mirrors of very low surface roughness with radii of curvature two orders of magnitude smaller than possible with superpolishing techniques [14]. The construction of very short cavities leads to low mode volumes inside the resonator and consequently to efficient optical interfaces between an ion and the resonator field. It is also very convenient that light can be coupled into and out of the cavity through the fibre cores wherefore no further optics are necessary. The central part of the Gaussian shaped mirror structure can be approximated by a sphere. For good resonant conditions, the wavefront curvature should match the spherical shape of the mirror to reduce clipping losses.

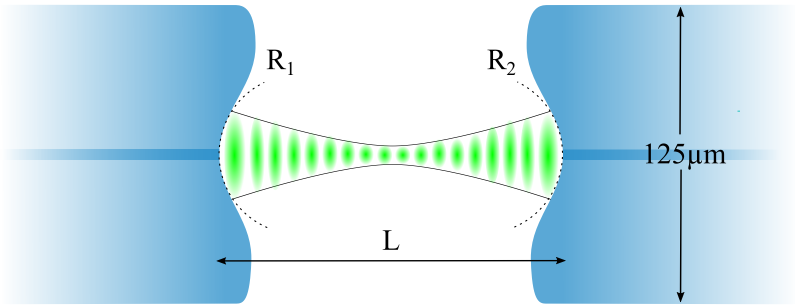

Figure 2.1.3: Sketch of a fibre cavity.

The transversal mode profile should be a Gaussian ground mode which has the lowest mode volume to built cavities with high finesse values. Multiple dielectric layers create coatings down to a transmission of 10 ppm allowing for fibre cavities with finesse values exceeding 60 000 [15]. The power coupling efficiency into the cavity mode is given by the overlap integral of the fibre mode and the resonator mode in the intersectional plane [16]. It therefore depends on the mode waists as well as the Rayleigh lengths of the light field inside the fibre and inside the cavity [17]. Thus, the coupling efficiency is maximized if the mode waist on the mirror w_m matches the mode waist of the light field inside the fibre. It is therefore favourable to not extend the distance between the two fibre mirrors to the stability limit, but keep the mode waist on the mirrors reasonably small to have large coupling efficiencies. Mode matching is claimed to be as high as 85 % for short fibre Fabry-Perot cavities [18] [19]. The geometric displacement between mirror structure and fibre core only effects the coupling efficiency but not the finesse of the resonator.

The geometry of such a fibre mirror is depicted in fig. 2.1.4. Calculations revealed that if a mirror structure is imprinted on a fibre end facet using a Gaussian laser beam, the useful mirror diameter D relates to the radius of curvature and structure depth as [18]

$$z_t \approx \frac{D^2}{8R}. \tag{2.1.9}$$

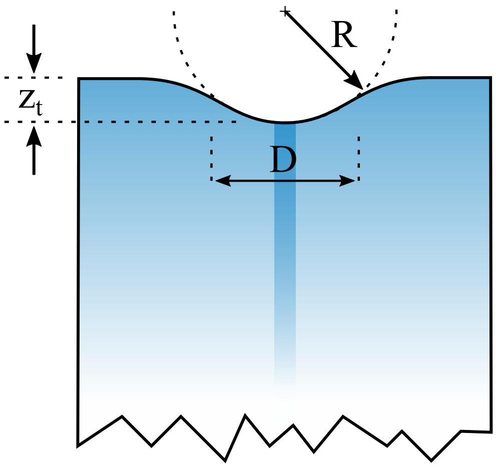

Figure 2.1.4: Geometries of a fibre mirror.

The useful mirror diameter D is defined as the full width up to which the $^1/_e$ Gaussian fraction coincides with the surface profile. This relation has been found true for fibre end facet machining with a CO_2 laser [18] during this work. Nevertheless, it might be more appropriate to define the useful mirror area as the part of the mirror structure up to where the spherical approximation matches the Gaussian fit. To optimize mode matching, it is also necessary that the mirror surface is orthogonal to the fibre core and that the offset between mirror centre and fibre core is negligible to achieve high coupling efficiencies. Please note that the *coupling rate* denotes the atom-photon interaction while the *coupling efficiency* describes the ability of coupling light through the fibre core into a cavity mode.

In the case of fibre cavities, the mirror size is restricted to the dimensions of the fibre and cannot be, per se, assumed to be sufficiently large. Clipping losses occur if the spherical wavefront curvature of the resonator mode does not match the mirror shape. The Gaussian mode profile has a spherical wavefront and a Gaussian intensity distribution and can hence be approximated for a single reflection by [18]

$$\mathcal{L} = \exp\left(-2\frac{(^D/_2)^2}{w_m^2}\right). \tag{2.1.10}$$

Practically, clipping losses are neglectable for spherical mirror diameters which measure at least 3 times the mode size on the mirror since then $\mathcal{L}(D = 6w_m) < 1\,\text{ppm}$.

2.2 Atom-Light Interaction

The interaction between a light field and an atom can be treated in the two-level approximation if the energy of a single photon of the light field corresponds to the optical transition of the atom. The interaction is said to be in the strong coupling limit if irreversible processes are much slower than reversible processes. This is, an emitted photon is much faster (re-)absorbed by the atom than it is lost. This regime is achievable for an atom placed inside an optical resonator which is resonant for the wavelength that equals the energy difference of the two state levels of the atom.

Thus, the above mentioned fibre resonators are frequently used for enhancing atom-light interactions and to study cavity quantum electrodynamics in its simplest form. The strong interaction between the light field and the atom is the key element of the state-readout process of a quantum state. The interaction between a two-level system and the quantized light field of the resonant mode was firstly desribed by the Jaynes-Cummings model [20]. The full quantum mechanical treatment of such a system can for example be found in [21].

Intuitively, it is favourable to place the atom in the minimal spot of the light field of a Gassuain ground mode intensity distribution to trigger the interaction as at that place the intensity is the highest. The coupling regime inside the cavity is quantified by the atom-photon coupling parameter g_0, the photon decay rate of the cavity κ and the non-resonant decay rate γ [22]. As the coupling parameter is $g_0 \propto d\sqrt{V_0}^{-1}$ where d is the optical dipole moment of the atom and V_0 the mode volume at the atom's place, it is possible to see how advantageous small mode volumes are. The smaller the mode volume or equivalently the shorter the cavity length, the larger the coupling rate between atom and photon. κ is the photon decay rate and the inverse of the photon lifetime in the cavity. The decay rate in the cavity is anti-proportional to the length and the finesse of the resonator. γ corresponds to non-resonant relaxation processes which lead to the loss of the photon out of the cavity volume. These losses comprise relaxations out of the two-level system, since under real conditions a two-level transition has always some small probability to decay into a third level. The cooperativity describes the ratio of the crucial coupling parameters [23]

$$C_0 = \frac{g_0^2}{2\kappa\gamma}. \tag{2.2.1}$$

and directly relates to the probability p_e of emitting a photon into the cavity mode as

$$p_e = \frac{2C_0}{2C_0 + 1}. \tag{2.2.2}$$

In practice to have reasonably high emission rates into the cavity mode, one aims for cooperativity values of the order one or larger, which is equal to the premise that $g^2 \approx \kappa\gamma$. Hence, if all three values are of the same order of magnitude, the photon emitted by the atom inside the cavity is caught between the two mirrors and is highly probable re-absorbed by the atom before it is lost. It also follows that the cooperativity is proportional to the finesse of the resonator which emphasizes the importance of resonators with large finesse values for the implementation of efficient optical interfaces. Hence, it requires resonators of highly reflecting low-loss mirrors and of short lengths. The latter requires mirrors with curvature of the same order of magnitude as the resonator length to built a stable resonator. To reach these values, the resonator shall have a length on the order of of 50 µm to 200 µm which necessitates mirror radius of curvatures of about 200 µm to 300 µm and finesse values of ideally 10 000 or higher. Eventually, one needs to compromise between cavity length and mode volume as both parameters contribute oppositely to the cooperativity. As it is possible to fabricate such small mirrors on fibre end facets, atom light coupling is intensively studied inside fibre cavities.

2.3 Ion traps with integrated cavity

Ion traps with an integrated fibre cavity are the practical implementation of stationary and flying quantum bits connected by an optical interface. For this purpose, ions with large dipole moments and suitable electronic ground state configurations are chosen. Ionisation is simple for hydrogen-like elements where one electron of the outer shell can easily be removed. The element Ytterbium is used in recent experiments as ^{171}Yb provides all necessary characteristics for studying light-atom interactions [24]. Ion traps are built inside ultra-high vacuum chambers to reduce refractive index fluctuations and the number of background collisions which kick the ion out of the trap. Oscillating electric fields trap charged atoms in a potential with a metastable saddle point in the center. This type of trap is called Paul trap and is further introduced in chapter 4. A cavity is brought into place such that the trapped ion is in the center of the cavity and the cavity is resonant to the desired dipole transition. This implementation of an optical interface using fibres simplifies the connection to existing networks for future information transfer. Conveniently, since the light field directly couples into the glass fibres, no further mode matching optics are required for light guidance. There also is the attempt to construct even more efficient interfaces by enlarging the mode matching between cavity mode and fibre mode by splicing parts of different fibre types to the mirror end [19]. The size of fibre cavities also leave a large optical access to the trapped ion for cooling and manipulation processes with additional laser beams.

The experimental benefit of ion traps has been demonstrated from multiple researchers leading to the ability to perform quantum operations on entangled ions [7, 25]. Figure 2.3.1 graphically shows a successful implementation of ion-light interfaces. If several of these traps are built, one aims to entangle the trapped ions and to demonstrate properties of quantum communication.

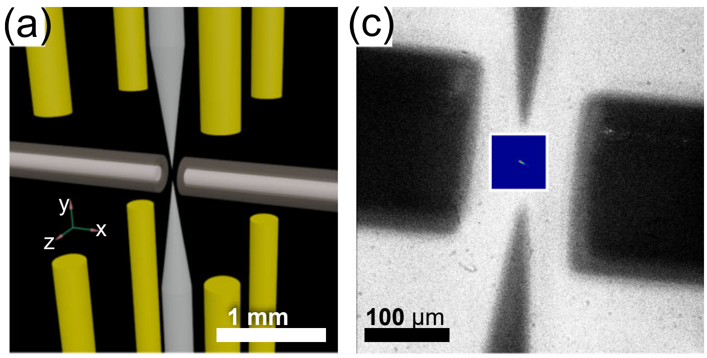

Figure 2.3.1: Pictures of needle Paul trap with ion cavity taken from [23]. (a) Ion trap with end cap electrodes (grey), compensation electrodes (yellow) and optical cavity (horizontal). (c) Shadow image with electrodes and fibres, fluorescence image of trapped Yb$^+$ ion.

CHAPTER 3

Fibre End Facet Machining

When exploring the physics of cavity quantum electrodynamics and the manipulation of quantum systems, it is very useful to work with resonator of certain geometries. Therefore, mirrors of well-chosen parameters for reaching in a favoured regime are required. The construction of a fibre end facet machining setup is therefore essential to adapt available fibre mirrors to experimental requirements in the facility of the *Universität Bonn*. This chapter provides an overview of the technical details concerning the constructed setup which has been built during this thesis. It also presents the important machining parameters and techniques which are essential to adapt the mirror geometries. Continuous improvements and renewal of elements from former experiments have significantly raised the achievable fibre mirror quality in the course of time.
The research groups of Prof. Jakob Reichel in Paris and Prof. Gerhard Rempe in Munich have also the ability of shaping fibre mirror surfaces. Both groups produce fibre mirrors in similar ways, using a CO_2 laser to create spherical structures on the fibre end facets. Especially the work of David Hunger [18], Sébastien Garcia [26], Konstantin Ott [27] as well as Manuel Uphoff [28] [29] provide useful information for the construction of a fibre mirror machining installation and the different ways of how to machine the fibres.

Glass fibres are made of silicon dioxide SiO_2 also named fused silica. The core of a fibre is made of doped silicon dioxide and the outer cladding of pure fused silica. This material has an high absorption index in the infrared region of light and therefore illuminating this material with light of a wavelength of $\lambda = 9.3\,\mu\mathrm{m}$ heats the outer layer and allows to shape the surface of the material. Evaporation and melting processes deform the substrate surface and the intensity profile of the laser beam is directly imprinted onto the surface structure. Fibre mirrors with a spherical shape are required for stable low-loss resonators. As a Gaussian profile can be approximate with a spherical central part, a Gaussian ground mode is employed for deforming the fibre surface. The ablation process is highly dependent on the deposited energy in the material surface and therefore the intensity profile and the pulse length of the laser beam have a significant influence on the final structure.

3.1 Setup Elements

The acousto-optic modulator (AOM) is the key element in the setup as it allows for the precise shaping of laser pulses. This element makes the pulse sequences adaptable to all sort of requirements and makes this setup much more advanced compared to the setups in Munich and in Paris. It prohibits the necessity of switching the laser on and off for pulse creation and enables to run the laser continuously at comparatively high duty cycles. An in-loop power control circuit comprising a fast photodetector and a proportional-integral-derivative (PID) controller shall guarantee the reproducibility of subsequent laser pulses. Finally, a hollow silica waveguide (HSW) cleans the Gaussian ground mode and mechanically creates beam pointing stability. A sketch of the setup is shown in figure 3.1.1 which comprises all necessary optical elements.

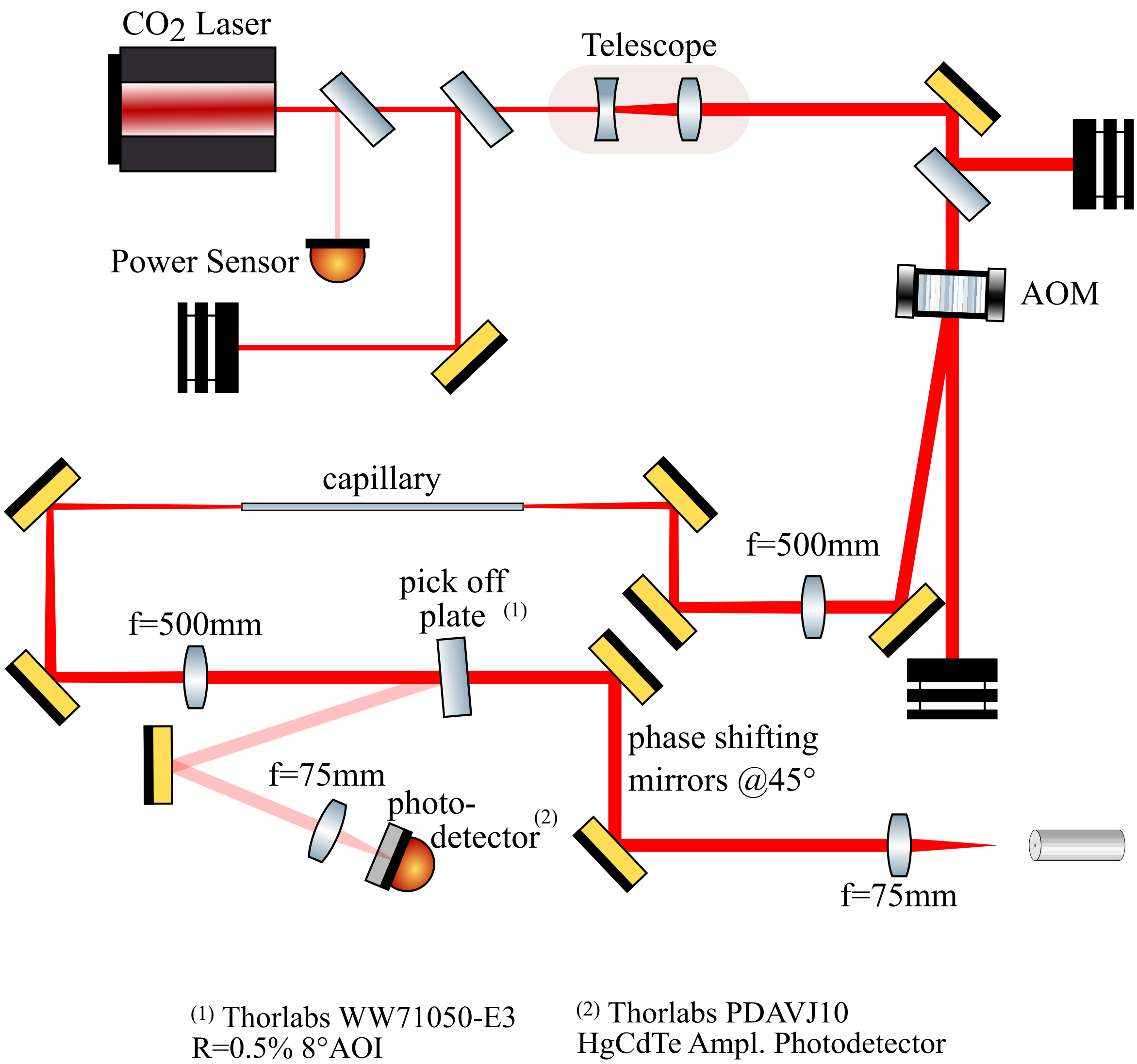

Figure 3.1.1: Fibre machining setup comprising all optical components for machining processes. The photodetector is part of an in-loop power control circuit which feds the AOM modulation power.

Laser and Duty Cycle
For ablation processes, a CO_2 laser with a maximum output power of 50 W at 100 % duty cycle is employed, emitting light at a wavelength of 9.3 µm which has been also used in the former machining setups built in the research group of Prof. Dieter Meschede. The laser is put on additional feet to lift the aperture and maintain the beam height at about 8 cm above the optical table in the entire setup. According to the manufacturer, the laser beam is horizontally polarized when exiting the laser aperture which matches the necessary polarisation direction of the implemented AOM. Just behind the aperture, a thermo power sensor[1] detects whether the laser is running. Two beamsplitters, one shortly behind the aperture and the other one behind the telescope, split the beam and deflect an important part of the intensity towards a beam dump. This allows to operate the laser at higher duty cycle and still have the right amount of laser power available for ablation processes. This is reasonable because the former master student found that the intrinsic power fluctuations decrease significantly for higher duty cycle [30]. Operating the laser at 20 % duty cycle corresponds to a total output power of 10 W of which a fraction of 2 W are transmitted through the AOM. The duty cycle has been chosen according to the required power for machining processes under the consideration of operating the AOM in the linear regime. At this configuration, up to 1.6 W can be deflected into the first order beam which corresponds to a diffraction efficiency of 80 %.

Acousto-optic modulator
The Germanium based acousto-optic modulator[2] (AOM) purchased with the corresponding driver[3] allows for analogue and digital modulation. The digital TTL signal is used as a digital shutter for the laser pulses and the analogue modulation is used for in-loop power stabilisation. Both, the analogue and the digital modulation can be addressed individually via the input-output card of the connected computer. The first order beam of the AOM is deflected and focussed into a hollow silica waveguide. The digital modulation of the AOM serves to shape the deflected beam to arbitrary pulse forms and does not have any restrictions on the pulse length or the repetition rate. In the former setup, the pulses were shaped using a mechanical shutter and turning the laser on and off accordingly. All operations were clocked with a 2 kHz rate and the pulse length could consequently only be adjusted in steps of 0.5 ms. The control circuit also allows to adjust the duty cycle without the need of repetitive power calibrations for fibre machining in case of changes in the direction or angle of the output laser beam. Only the waveguide coupling has to be adjusted in this case. Changes in the coupling efficiency due to intrinsic beam pointing fluctuations shall be compensated with the control circuit.

Waveguide
A hollow waveguide[4] is the equivalent of an optical glass fibre but for mid to far infrared applications, see figure 3.1.2. The waveguide measures roughly 20 cm and is employed for two reasons. Firstly, at this length, higher order modes are highly sup-

[1] µW Power Sensor for MID-IR Laser beams: `www.lasnix.com/datasheets/power-sensor`
[2] I-M041-10C11V41-P5-GH7 from Gooch & Housego
[3] HP041-125ADG-A10 from Gooch & Housego
[4] `www.lasercomponents.com/de-en/product/fibers-for-co2-and-eryag/`

pressed and a clean Gaussian ground mode is expected as output mode behind the capillary. Secondly, the waveguide is mechanically fixed and shall prevent the beam pointing from moving spatially over time due to fluctuations in the refractive index or intrinsic beam pointing fluctuations coming from the laser itself during shooting processes. Since fused silica glass has a high absorption coefficient for light of wavelengths larger than 2.1 µm, it prohibits the employment of glass fibres for guiding light of a wavelength of 9.3 µm. For far infrared applications, such a waveguide is a hollow fused silica capillary with a diameter of 1 mm having an optically reflective internal silver halide coating which guides the light field along propagation direction. Coupling into a

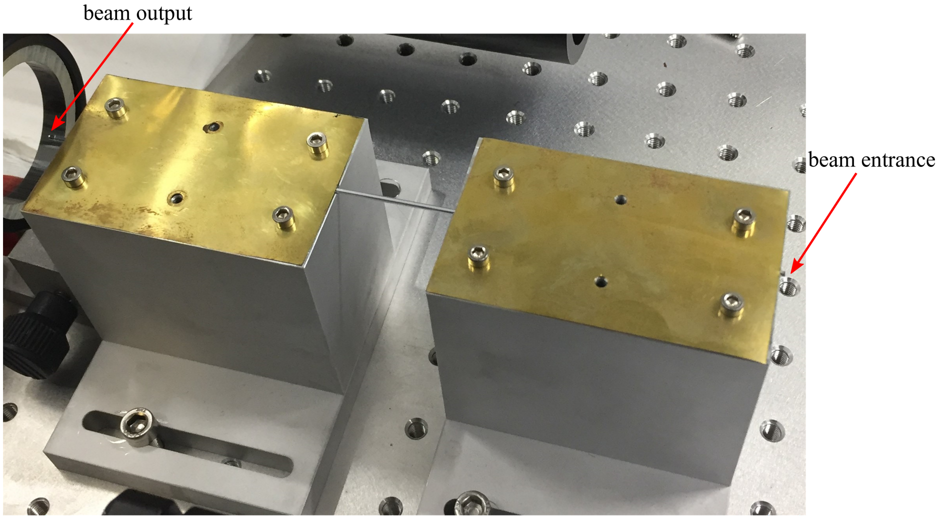

Figure 3.1.2: Picture of hollow silica waveguide in the setup clamped onto a custom v-groove.

waveguide is comparable to coupling a light beam into an optical glass fibre. However, no fibre couplers are used and a lens with a focal length of 500 mm is employed. The two mirrors required for efficient coupling are placed between the focussing coupling lens and the waveguide entry. The lens focusses the laser beam to a calculated diameter of 740 mm. The manufacturer recommends a mode waist corresponding to 65 % to 70 % of the waveguide's size for best coupling performance. Also, lenses with an f-number larger than 20 are recommended, which is the case for an one inch lens and a beam of 8 mm $^1/_e$ diameter. If the smallest achievable beam waist is too large for a specific lens, one risks to burn the cleaved end of the waveguide. But if the beam waist is too narrow, higher order modes are heavily exited and the output intensity profile corresponds to a superposition of multiple transversal modes. This effect has been seen for a lens with a focal length of 200 mm which has been used for the first coupling attempts. In the current configuration, the beam waist at the entrance of the capillary is slightly larger than the recommendation and a lens with a focal length of 450 mm would be more suitable. However, the number of available optics is very limited for infrared applications and such a lens needs to be customized. This is the reason why a coupling lens with a focal length of 450 mm is not used. In case more power is required for machining processes, this lens should either be replaced by a shorter one or a second lens must be added to prevent burning the capillary entrance. Behind the capillary, a second lens with a focal length of 500 mm is collimating the diverging output beam whose exit divergence is assumed to be equivalent to the input divergence.

Polarisation Modulation
The phase shifting mirrors[5] which transform the linearly polarized laser beam into a circularly polarized one are transfered from the former setup build by Michael Kubsita during his Master thesis to the new one. It has been found that mirror structures that have been produced with circularly polarized light show less ellipticity than those structures machined with linearly polarised light [28]. The polarisation ellipticity of the beam was determined with a linear polariser behind the phase shifting mirrors. For this setup, the ellipticity was found to be

$$\epsilon = 1 - \frac{P_{\max} - P_{\min}}{P_{\max} + P_{\min}} = 0.90. \tag{3.1.1}$$

Inducing a phase shift of $\lambda/4$ transforming the polarisation from linearly to circularly is usually done with a $\lambda/4$ plate, but as there exist no $\lambda/4$ plates for infrared applications, the polarisation change is achieved by two 45° reflections from tilted mirror surfaces with an adapted coating. The beam is reflected from the mirror surfaces at an angle of incidence of 45° with respect to the incident polarisation axis which tilts the polarisation axis for every reflection. The height of the beam is by doing so increased by 7 cm and adapted to the placement of the existing white-light interferometer and translation stage at a height of 15 cm above the optical table. The final lens with a focal length of 75 mm focuses the infrared laser beam down to a beam waist of 50 µm.

3.2 Machining Elements

Except for rebuilding and aligning the setup itself, there are a few essential components that have been designed and modified for efficient fibre machining. The production of a fibre mirror requires the perpendicular alignment of the cleaved fibre end facet to the interferometer objective prior to shooting processes. The fibre is then moved with the translation stage about 8 cm in horizontal direction into the laser beam axis. After applying the desired pulse sequence to the fibre surface, the fibre is moved back to the interferometer and the machined surface can be reconstructed with interferometric images using Fourier evaluation, see [30]. The white-light interferometer and the evaluation script for surface reconstruction has been built and written by Jose Gallego and Michael Kubista. If this is done for all fibres in the holder, the holder is placed into a coating disk which is sent to the coating company *LaserOptik GmbH Garbsen* where a high reflectance coating is evaporated on the spherical fibre surfaces.

Researchers [26] have tried to describe the evaporation and melting process with analytically calculable thermodynamic equations. However, experiments have shown that these calculations do apply to ablation processes on SiO_2 glass plates, but not on fibre end facets. Similarly, it has also been found that on glass plates the structure depth depends linearly on the pulse duration, but certainly not to fibres [29]. Consequently, no calculations have been conducted to choose the optimal intensity and pulse length configurations for a desired mirror shape. It has also been found that

[5] `https://www.lasercomponents.com/de-en/product/phase-shifting-mirrors/`

fibres for different wavelengths behave quite differently for the same pulse sequence. The doped core of the fibre seems to melt at higher intensities than the outer pure silica cladding. Changes in the doping of the glass lead to non-neglectable necessity of adapting the pulse sequence for achieving similar structures.

Fibre Holder

The old fibre holder is replaced by a new one which has been fabricated by the workshop of the *Physikalisches Institut der Universität Bonn* which serves to arrange, machine and coat the fibre surfaces. The design has been adapted from the holder developed by Hendrik Meyer and Matthias Steiner during their PhD thesis in collaboration with the group of Prof. Jakob Reichel. The fibres are placed into the holder prior to machining and are removed after coating. A total number of 26 fibres have space in the new holder of which 24 fibres are accessible for shooting processes due to the limitation of the translation stage. A spacing of 2 mm between two neighbouring fibres and a three-point bearing provide a defined placement of the fibres in the holder. Figure 3.2.1 shows a sketch of the holder geometries. Grooves of cylindrical indentation with a radius of 100 µm hold by a spring on top were found machinable and very convenient for clamping the fibres. The holder fits into the laser setup, see figure 3.2.2 as well as into the coating disks adapted to the coating chambers at *LaserOptik GmbH Garbsen*.

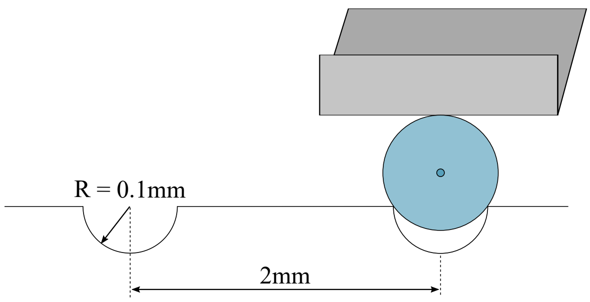

Figure 3.2.1: Sketch of fibre holder (not to scale) fabricated by the fine mechanical workshop of the *Physikalisches Institut*. It offers a theoretic three-point bearing for 26 fibres with a 125 µm cladding diameter.

The high cleave quality of fibres with acrylic coating combined with the precise machining of the grooves immensely reduce the aligning process of the fibres in front of the interferometer, compared to the former one. Unfortunately, this is not completely true for copper fibres which might be due to the suboptimal cleaving quality or the flexibility of the copper fibres in general. Copper fibres require additional alignment to ensure the perpendicular orientation of the surface with respect to the interferometer. Nevertheless, the new fibre holder significantly accelerates the machining process for acrylic and copper coated fibres. There also was the attempt of building fibre holders with chemically edged grooves which are commercially available from the company *OZ Optics*. Since the straightness of this holder was equally good, the fibre holders machined by the workshop were chosen for time and financial reasons.

Graphical User Interface

The Graphical User Interface written in Matlab's appdesigner is the heart of the fibre machining setup and has been adapted from the former experiment to the current

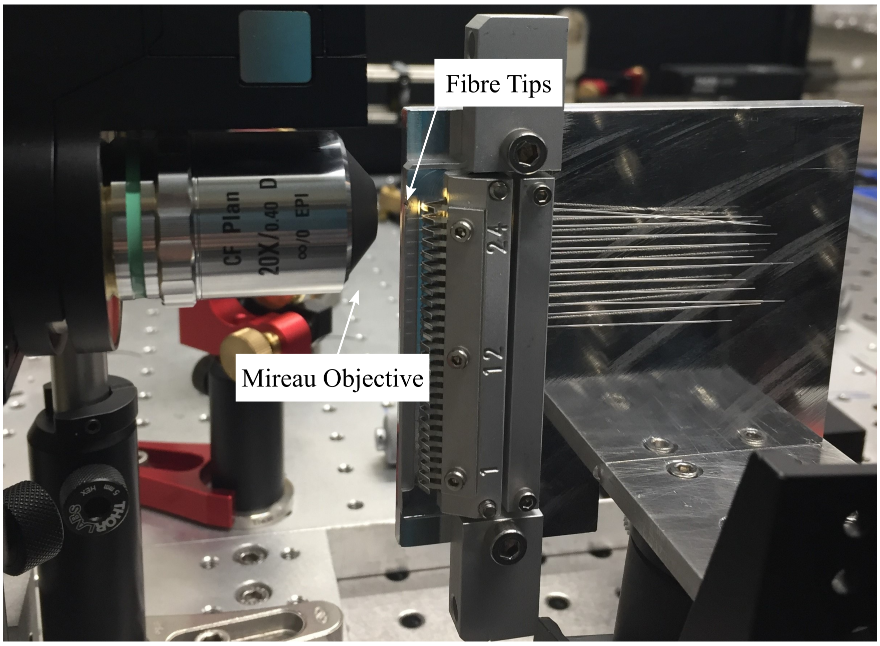

Figure 3.2.2: Picture of the fibre holder in front of the Mireau objective of the interferometer.

setup, see figure 3.2.3. The part of the interface concerning the pulse sequence has been modified, all other parts relating to the interferometer and the stage control are left unchanged. The box entitled *Interferometer* is essential for the alignment and analysis of fibre end facets. The surface of a fibre can be observed through a camera integrated in the interferometer and multiple interferometric pictures allow for the reconstruction of the fibre surface using Fourier analysis. Please refer to the master thesis of Michael Kubista [30] for further information about these functionalities and the software that enables surface reconstruction.

In the lower left part, the user can now select pulse lengths of arbitrary times in units of milliseconds, the number of pulses and the signal voltage value which corresponds to the power in one pulse. All alignment and calibration was conducted for a duty cycle of 20 % and it is currently possible to produce pulses with a maximum power of 1.6 W. This can generally be changed if more power is required. Since the intrinsic beam pointing of the laser might change with different duty cycle values, especially the waveguide coupling has to be considered and adjusted.

The interface allows to choose between *single shot* and *multi shot*. When pushing the button *Shoot*, the user is asked to enter a unique fibre name in whose folder all the information of the machining process is stored. It creates pulses with a Gaussian rise and fall slope of 5 µs and a constant interspacing part, lasting for the time specified by *Pulse Length* in units of milliseconds. Pulses are produced as often as specified with *Number of Pulses* with a total power adjustable with *Signal Voltage*. A time lag of 1.5 s separates two subsequent pulses from each other. This technique is called *single shot* in the following sections.
The *Multishoot* button also releases a shooting process with multiple pulses. The main difference is that the fibre surface is moved in transversal direction between two

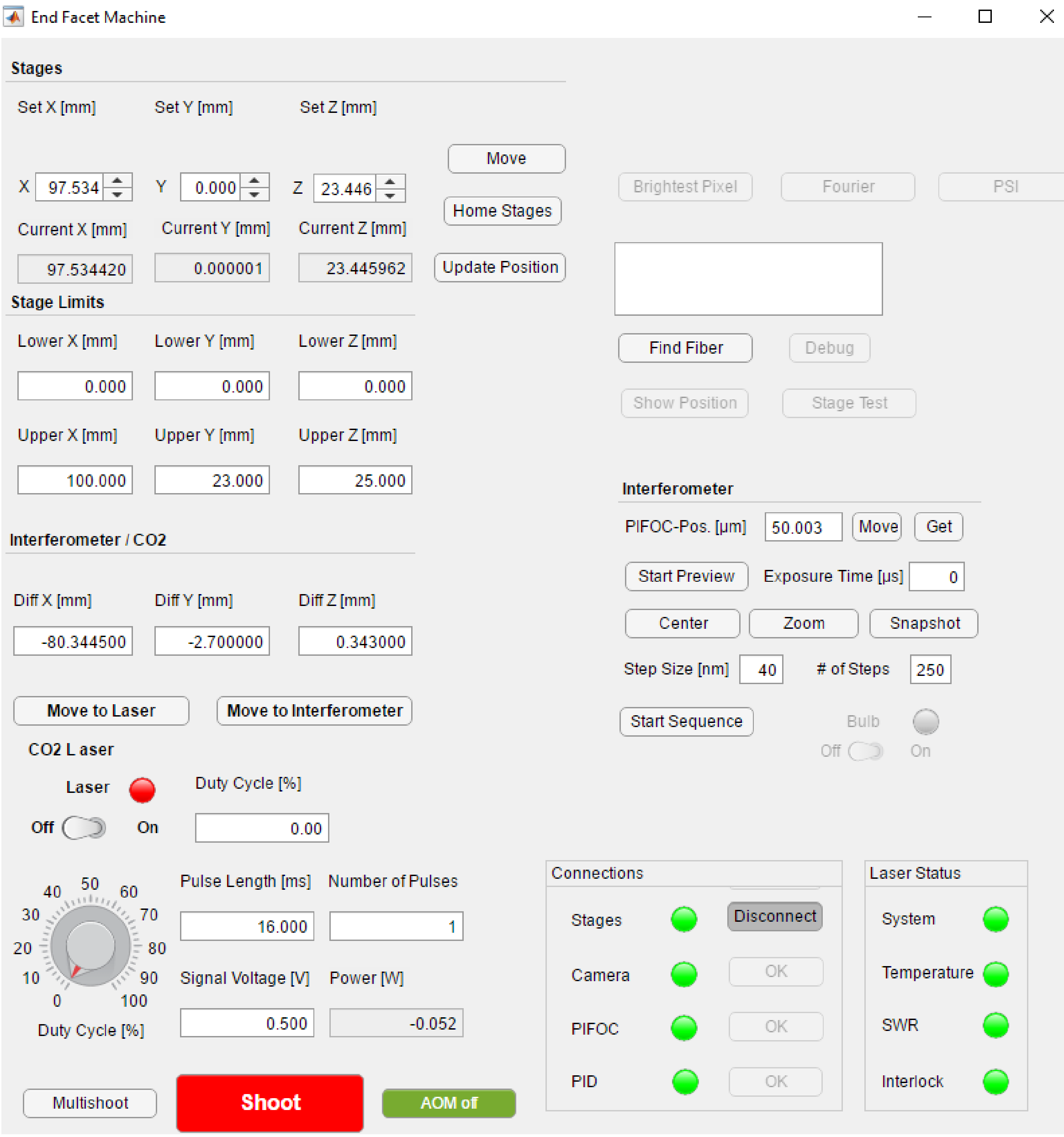

Figure 3.2.3: Modified graphical user interface for machining processes.

subsequent pulses which allows for the creation of larger structures and the control of ellipticity. This machining technique requires a file which contains relative coordinates in units of µm for indicating the position of each pulse centre relative to the next one. Pulses should be applied in concentric circles around the fibre core, starting with the outermost points and ending in the center. One point is ought to be skipped between two neighbouring points as it has been found advantageous by another research group [26]. This process is further named *multi shot*. So far, the relative coordinates for stage movement are generated in an external script and saved in a text file. For better handling, this script could be implemented in the main machining interface.

The user interface also enables to turn the AOM on and to run it at constant power by the use of the green *AOM off* button. The label turns into *AOM on* if the AOM is powered. The fraction of the power deflected into the first order beam is proportional to the value entered in *Signal Voltage*. This functionality shouldn't be used for any machining processes but for alignment and calibration only.

Beam Waist Selection

The waist of the laser beam which shapes the fibre surface can be adjusted by moving the fibre end facet along the propagation axis of the laser beam, see figure 3.2.4. Calibrations enable to select a specific beam waist for every fibre individually. During this work, it was found that working with a beam waist exceeding the fibre's diameter is favourable. The central spherical part is enlarging with larger beam waist, but the same does also apply to the edge rounding. Edge rounding means that the edges of the cleaved surface melt and a defined border vanishes. Eventually, one needs to compromise between spherical diameter and edge rounding when using the *single shot technique*. The effect of edge melting can be reduced by applying a pulse sequence to different points on the fibre end facet (cf. *multi shot*) using less power and shorter pulses.

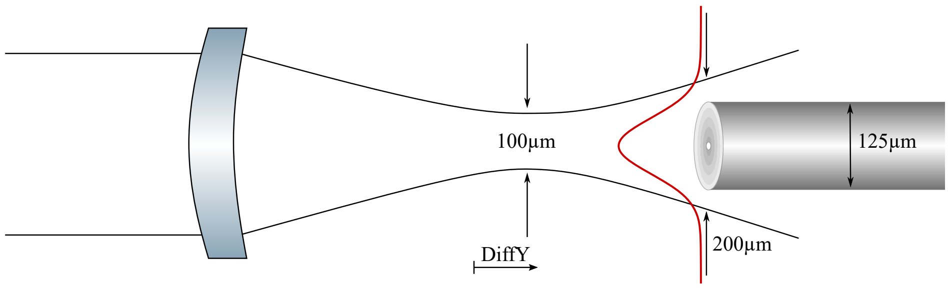

Figure 3.2.4: Sketch of how to vary the beam waist at the position of the machined fibres and intensity for machining processes.

Beam waists between 50 µm and 1 mm can be selected for machining processes, see figure 3.2.5. In the GUI, the *DiffY* value which is defined as the difference between the focus of the interferometer and the waist position of the laser beam needs to be adjusted accordingly. Figure 3.2.5 shows the horizontal and vertical beam waist measured with the knife edge method. For this, a knife edge is moved horizontally and vertically through the beam profile and the transmitted power for different knife edge positions is recorded. The curve follows an error function as expected for a Gaussian intensity profile. From the fit to the data points the beam waist can be determined. The accuracy of this measurement might not be too accurate, due to the lack of power stabilisation, see below, and significant power fluctuations of the employed power meter. This is, two subsequent waist measurements do not always result in the same beam waist. The errors on the data points solely arise from the fit and do not take the mentioned fluctuations into account. In principle, it is possible to use waist sizes larger than visible on the graph. But when selecting beam waists of 1 mm or larger, one should always consider the spacing between two neighbouring fibres and the risk of affecting these with such large beam waists.

In-loop Power Control Circuit

The reproducibility of subsequent machining pulses ought to be well monitored. For this reason, a control circuit comprising a photodetector and a proportional, integral

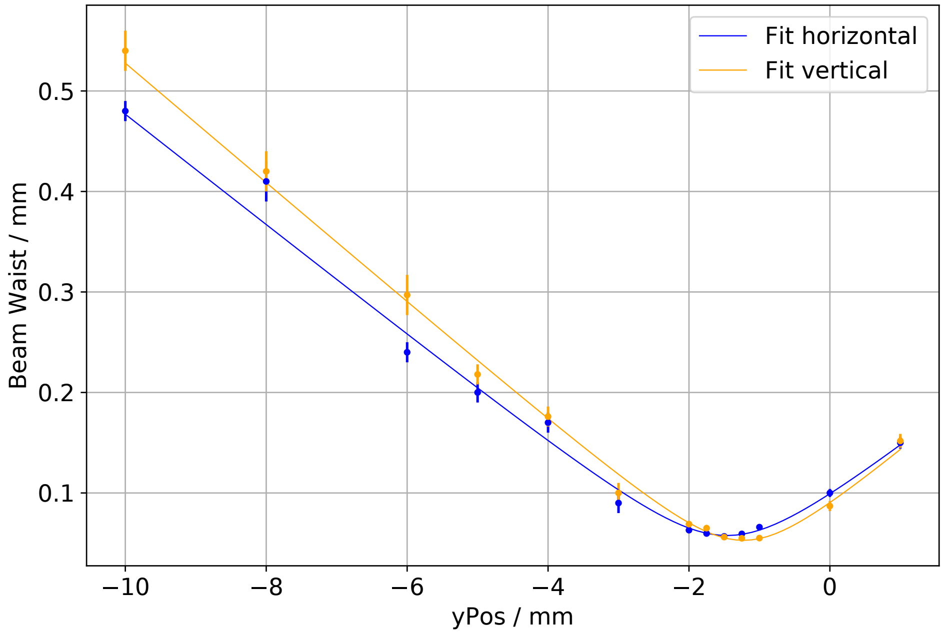

Figure 3.2.5: Measurement of beam waist using the knife edge method for different positions along propagation axis. Calibration for shooting processes.

and derivative (PID) controller which feeds the AOM power modulation has been implemented. To prevent the AOM controller from any damage due to high voltages, the PID controller has to be modified to 0 V to 10 V output voltage. A fast HgCdTe amplified photodetector[6] detects all in-loop power fluctuations with a 100 MHz resolution. A wedged window[7] which shall deflect 0.5 % of the incident power at an angle of incidence of 8° towards the photodetector is placed before the phase shifting mirrors. This percentage of deflection was found not accurate for this setting. It seems that much less power is deflected from the wedged window. Fluctuations on a timescale of µs become observable on the photodetector. The intrinsic power fluctuations due to a duty cycle of only 20 % are clearly visible. Regular intensity patterns repeat every 20 µs, see figure 3.2.6 having features on the 1 µs scale which change for different duty cycles. In principle these fluctuations should vanish for a duty cycle of 100 % but the setup is currently not suitable for running at maximum power. Moreover, the employed PID controller has a bandwidth of several MHz and can reduce but not completely compensate for these fast duty cycle changes. Nevertheless, thermal ablation should not be affected by fast fluctuation, and only power instabilities over several milliseconds play an important role.
The unfavourable properties of the wedged window become visible in the graph of figure 3.2.6. It shows the photodetector's output signal for no in-loop power control, modulating the AOM with constant power. In theory, the detected signal should fluctuate in intensity but always showing the same specific duty cycle pattern when the overall power changes. The three different curves show the laser signal on the detector at different times without changing the power of the AOM. The mean voltage of the signal drifts heavily within a time of 20 ms as well as the shape features. On the same time, the power measured with a second power meter with low resolution in the system

[6] item PDAVJ10 from Thorlabs
[7] item WW71050-E3 from Thorlabs

does not significantly deviate from its mean value. This suggests fluctuations of the polarisation orientation of the laser beam and consequently a change of the picked off power by the wedged window. This is the reason why the control circuit, as it is currently implemented, does not work.

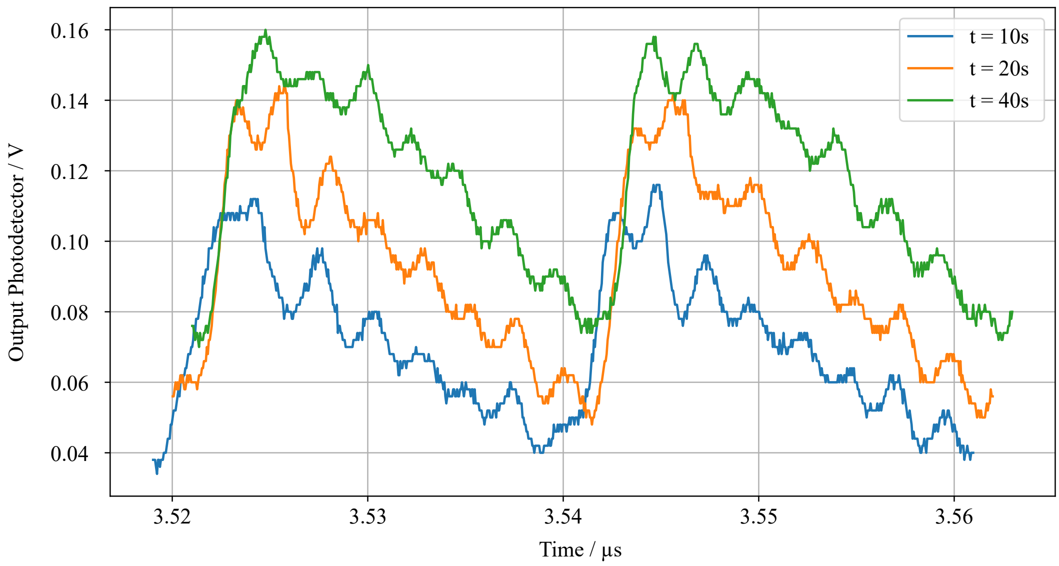

Figure 3.2.6: Observable duty cycle on fast photodetector. One cycles lasts 20 µs, signal of photodetector changes over time for constant AOM power whereas the power in the system is measured to be almost constant. The huge differences are likely due to polarisation fluctuations of the incident laser beam and prohibit the functioning of the power control loop.

The manufacturer does not provide any details about the polarisation dependence of the wedged window employed for power stabilisation, but this dependence can be experimentally demonstrated. The behaviour of the control circuit was analysed by monitoring the power in the fibre machining path while the control circuit was operating. Concretely, a thermal power meter[8] from Coherent with a specified rise time of 10 ms was put at the place where usually fibres are shaped. If a polariser is inserted into the laser beam between outcoupling lens and wedged window, the polarization extinction ratio (PER) can be measured to be 49.5 dB which demonstrates to a very good extent horizontal polarisation. Doing so, the signal on the photodetector decreases which shows a dependence of the polarisation of the wedged window. It seems that the pick-off plate does significantly deflect power of other than horizontally polarised light. This property is a severe problem for power stabilisation, see figure 3.2.7. The figure shows the time dependence of the power in the system with in-loop control circuit and without it. Running the AOM at a constant power is more stable than controlling the AOM power with the PID output of the control circuit. The measurement also confirms the choice of the duty cycle leading to constant laser output power and suggests that beam pointing fluctuations coming from the laser is insignificant.

[8] PowerMax Pro 150F HD

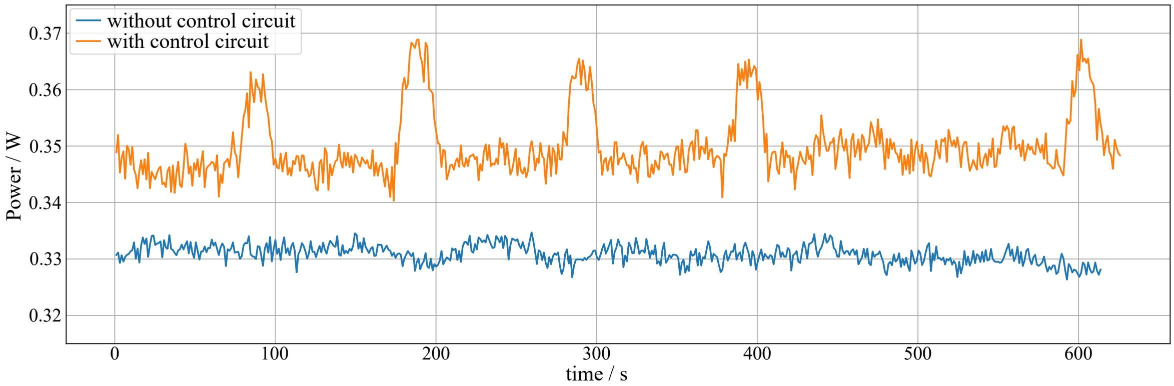

Figure 3.2.7: Power measured at the position of the fibre for 10 min with and without the control circuit including PID controller. It demonstrates the failure of the PID control loop for power stabilisation.

As the percentage of the deflected light from the wedged window is very small, it is very sensitive to polarisation fluctuations. The polarisation dependence of the wedged window was already suggested before [30] while setting the Lasnix Power Sensor in the former setup. In future, the problem could be solved by introducing a Brewster plate which cleans the polarisation of the laser beam before picking off the power. Also, the wedge window should be replaced by a beam splitter with a ratio of 50:50 for reflection and transmission for both p- and s-polarised light to further lower any polarisation dependence. Since the control circuit artificially induces more power changes than there intrinsically exist, the pulses for surface machining are created without any control circuit. Figure 3.2.8 graphically shows the power distribution over time for pulses with and without control circuit. The AOM power is modulated for pulse creation with the same signal as it is generated for the PID control signal, except for the "height" of the pulse. It was found that for both single shot and multi shot technique, the power in each pulse is stable enough for the production of spherical fibre end facets.

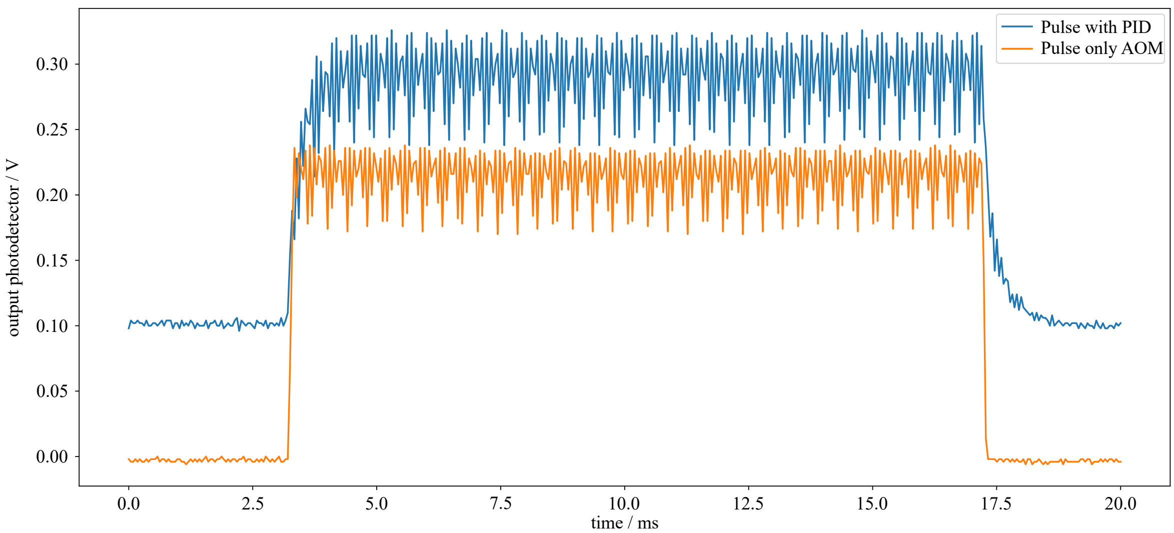

Figure 3.2.8: Pulse shape for fibre machining with PID controller and without. The blue curve has a vertical offset of 0.1 V.

3.3 Results

The work during the last year has contributed to the technical knowledge for the fabrication of fibre mirror. The setup has been successfully built and the user interface adapted such that it is suitable for customized usage. Additionally, a large number of fibres have been successfully fabricated and the fibre tips have been coated with high-reflection layers. After going through the entire machining process, it was possible to built a fibre cavity and to show that the measured finesse of the resonator is in accordance with the expectation values.

3.3.1 Criteria for Mirror Geometries

A total number of roughly 140 fibre mirrors of three fibre types have been produced: SM2000 and FG050LGA fibres from Thorlabs and CU600 fibres from IVG fibres. Since these fibres are supposed to be used in a soon built experiment, improved version of [31], they are coated for a wavelength 1988 nm with a transmission of $\mathcal{T} = (160 \pm 50)$ ppm for an angle of incidence of 0°. The core of SM2000 fibres measures 10 µm and the mode waist on the mirror surface measures roughly 11 µm for a cavity of the length of 300 µm. This is why mirror structures with spherical shape over a diameter of 60 µm are required for ensuring low clipping losses at this wavelength. For the realisation of these geometries elaborated techniques are used. The applied coating is also high reflective for a wavelength of 670 nm as the same destructive and constructive interference conditions apply to $1/3$ of the design wavelength. For this purpose, also CU600 single mode fibres have been machined whose core measures only 5 µm. Consequently, mirror structures of 30 µm diameter are large enough for this wavelength. Thus, the requirements for the mirror geometries for the three different fibre types differ from each other.

3.3.2 Cleaving Fibres

Prior to any machining processes, fibres have to be prepared, cleaned with isopropyl alcohol and cleaved. The new AutoCleaver S1 from Nyfors was found very suitable for the SM2000 and FC050LGA fibres with UV cured acrylate coating but certainly not for CU600 fibres. The latter copper fibres require an additional treatment prior to cleaving. It is essential to remove the carbon layer before cleaving to produce surfaces with low cleaving angles.
The Nyfors AutoCleaver S1[9] from *Fujikura* has shown huge improvements in cleaving qualities upon the former High Precision Fiber Cleaver CT-30 series. The manufacturer predicts cleaving angles below 0.3° and very flat end facets for the AutoCleaver. The work with it confirms these claims for fibres with acrylate cladding, e.g. SM 2000 fibres from Thorlabs, but not for fibres with copper coating. It appears that copper fibres from IVG[10] are not very suitable for this cleaver. Most cleaving attempts fail and raise the error message "**Fiber slipping?**" in the AutoCleaver software. It is also not possible to splice these fibres afterwards since the fibre's surfaces exceed the

[9] `www.fusionsplicer.fujikura.com/products/fiber/cutting/details/2039948_10189.html`
[10] `www.ivgfiber.com`

tolerable cleaving angle. Copper fibres are very flexible and suitable for high-vacuum applications but require additional treatment prior to cleaving.
Before cleaving copper fibres, the outer copper coating is chemically etched away. The fibres are therefore soaked in 40 % concentrated ferric chloride $FeCl_3$ for around 10 min which completely removes the copper layer. After thorough cleaning with isopropyl alcohol, the cladding of the fibres is still covered by a thin carbon layer which cannot be easily removed. It can be assumed that the carbon layer below the copper coating causes the problems with the present cleaver. Carbon is a lubricant and prohibits proper mechanical clamping of the fibre tip. However, proper clamping is essential for the cleaver since the high tension of the fibre leads to high quality cleaves.
There have been a few attempts of removing this carbon layer. Chemical removal would be advantageous since this should neither cause any mechanical damages to the glass nor make it porous. For this reason, copper fibres from IVG have been soaked in multiple acids, this is

- 95 % sulphuric acid
- aqua regia, a mixture of nitric acid and hydrochloric acid
- piranha solution, a mixture of sulphuric acid and hydrogen peroxide

but none of these liquids removed the carbon layer. Eventually, the carbon has been burned which poses a challenge to the stability and intactness of the glass fibre. The heating process is very subtle. The specifications allow a maximum temperature of 400° for times exceeding 60 s and fibres which have been exposed to too much heat break during the cleaving process. It has been shown that using a gastronomic burner turned to small flames can carefully burn the carbon layer. Keeping a minimum distance of 4 cm between flame and fibre is recommended. Being patient and leaving time to the process is also advantageous. Only the fibre end is freed from carbon to ensure proper clamping and reduce the risk of fibre damage. Figure 3.3.1 shows a sketch of the topview onto the AutoCleaver for copper fibre cleaving. The cleaved fibre tip is still covered with a carbon layer after cleaving. Especially when working with high voltages, keep in mind that a copper layer remains on the fibre tip. Surely the machining process with the CO_2 laser burns a part of the carbon layer but certainly not removes it entirely.

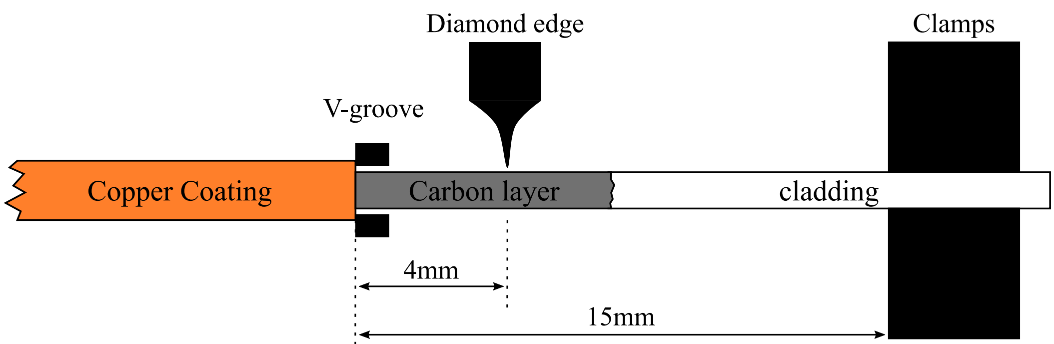

Figure 3.3.1: Topview on Nyfors AutoCleaver S1 with copper fibre. At the tip of the fibre the carbon layer has been burned. The cleaved fibre end is still covered with a carbon layer.

The fibres are cut into 10 cm pieces to properly store them onto the disk in the coating chamber. Consequently, all fibres have to be spliced to another fibre piece before working with them. The two fibre types suitable for a wavelength of 2000 µm can be seen in figure 3.3.2 where the different core sizes are clearly visible.

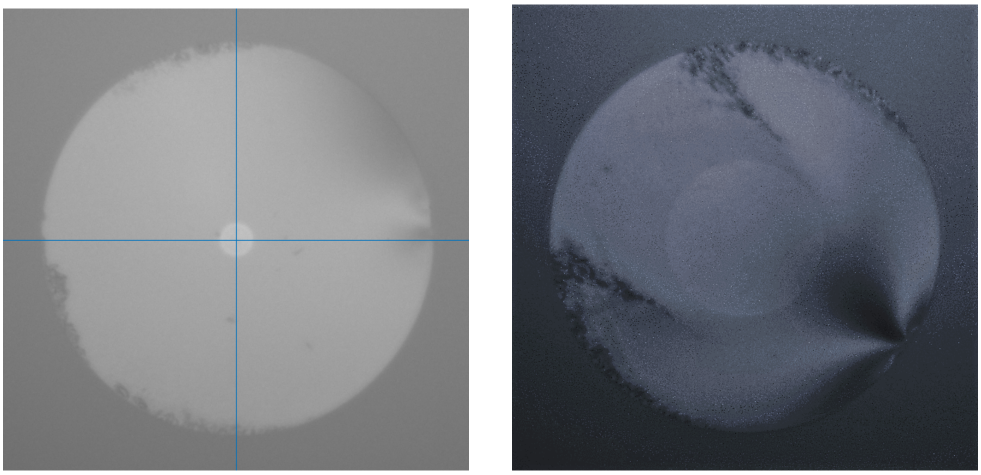

(a) SM2000 fibre with illuminated 10 µm core in the center.

(b) Multimode fibre FG050LGA with 50 µm core visible.

Figure 3.3.2: Cleaved fibre end facets seen through the white-light interferometer.

3.3.3 Pulse Sequence

The fibres are shaped with beam waists between 200 µm and 220 µm using laser pulses with a power of 640 mW to 800 mW. Depending on using single pulses or multiple pulses, the duration is between 16 ms and 35 ms. The higher the number of pulses, the shorter the pulses for achieving similar geometries. It has been found that the total power influences the radius of the structure while the pulse duration rather modifies the depth of structure.

Employing multiple pulses is beneficial in comparison to single pulses. This is, less power is required and the precise centring around the fibre core is enhanced. Also, multiple pulses correct for defects of bad cleaves. With single pulses every little feature on the cleaved surface coming from the cleave itself or some dirt deposited on the surface is directly imprinted on the resulting mirror structure, while multiple pulses do compensate this effect to some extend. It is possible to create spherical structures with diameters up to 40 µm with single pulses of 220 µm in diameter. It is also possible to compensate decentration of the structure ”by eye” by placing a second pulse off centre in the opposite direction. The geometries achievable with single pulses do fulfil the requirements for resonators of wavelengths in the visible electromagnetic spectrum.

The effect of edge melting can be restricted when employing multiple pulses. The lower energy deposition and heat dissipation causes less edge rounding and enlarge the spherical central part. There were a few attempts of placing the pulses at different radii around the core, with different numbers of pulses and consequently various of powers and pulse lengths are used. Good results are achieved for 25 points at 8 µm and 16 µm around the core. Even larger structures can be achieved for 46 points at

radii of 10 µm and 20 µm with a time delay of 1.5 s between two subsequent pulses. If one aims for elliptical structures, the points should be placed elliptically around the core. The roundness of the structures can be compensated by this technique by placing the pulse on circles perpendicularly to the transversal mode ellipticity. Please do not confuse with the ellipticity polarisation of the laser beam.
There is one element in the setup, either the waveguide, the outcoupling lens or the wedged window, which shifts the beam center severely when working at higher intensities. The center moves by almost 1 cm for a path length of roughly 1 m for powers exceeding 1 W. Likewise, as soon as power values larger than 1 W are used, the precise localisation of the beam centre on the glass surface is not possible. Figure 3.3.3 shows the dependence between analogue AOM modulation voltage (entered in the *Signal Voltage* field in the GUI) and the power at the position of the fibre. It suggests a linear regime only over a restricted area. If measuring the power directly behind the capillary, the linearity extends up to 8 V analogue modulation. Above a certain threshold, it is not possible to precisely measure the total power. The reason is that the power meter is put into the diverging beam and for large intensities not all power can be captured. Additionally, as the beam centre shift extremely, the beam drifts partly off the detector's head. Due to the lack of space, this cannot be changed easily. To prevent any thermal effects to restrict the centring of mirror structures, machining powers are kept below 800 mW in the linear regime. If one needs to work at higher power, this problem needs to be investigated first.

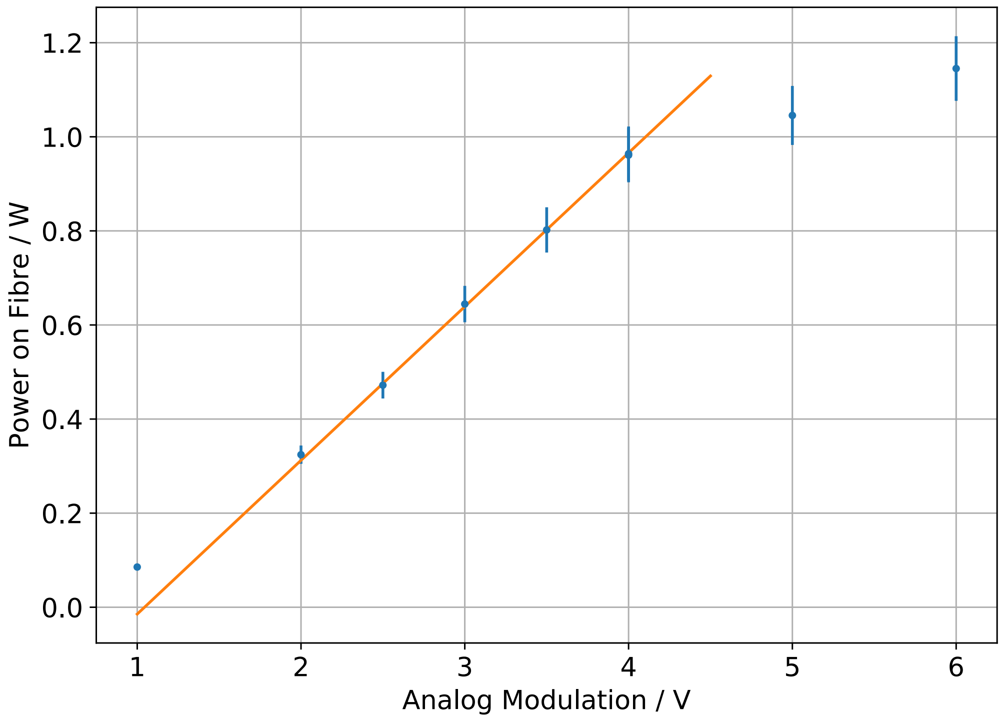

Figure 3.3.3: Power calibration data for fibre ablation processes. Data points in blue. Fit curve in linear regime indicated by the line calculated to be $P = (0.327 \pm 0.006)\,\mathrm{W/V} - (0.341 \pm 0.020)\,\mathrm{W}$. Linear regime only between $P = (300 - 1000)$mW. Above 1 W thermal effects prohibit proper calibration of total power.

3.3.4 Analysis of Obtained Structures

Analysis using Interferometric Data

The white light interferometer is very useful to examine the created structures in terms of depth and overall shape. It allows for the reconstruction of the fibre surface and the estimation of the radius of curvature by fitting a Gaussian and spherical function to the central part of the structure. The white-light interferometer is used as it has been built from the former student.
Figure 3.3.4 shows the interferometric picture of a machined SM2000 fibre surface. A total number of 46 pulses with a pulse length of $\tau = 16.5\,\mathrm{ms}$ and a power of $(794 \pm 20)\,\mathrm{mW}$ have been used. The dots on the picture indicate the position of the individual laser pulses on concentric circles around the core with a diameter of 20 µm and 40 µm. A border of 15 µm is melted away and reduces the total fibre surface. The spherical structure takes a diameter of 60 µm on the remaining surface.

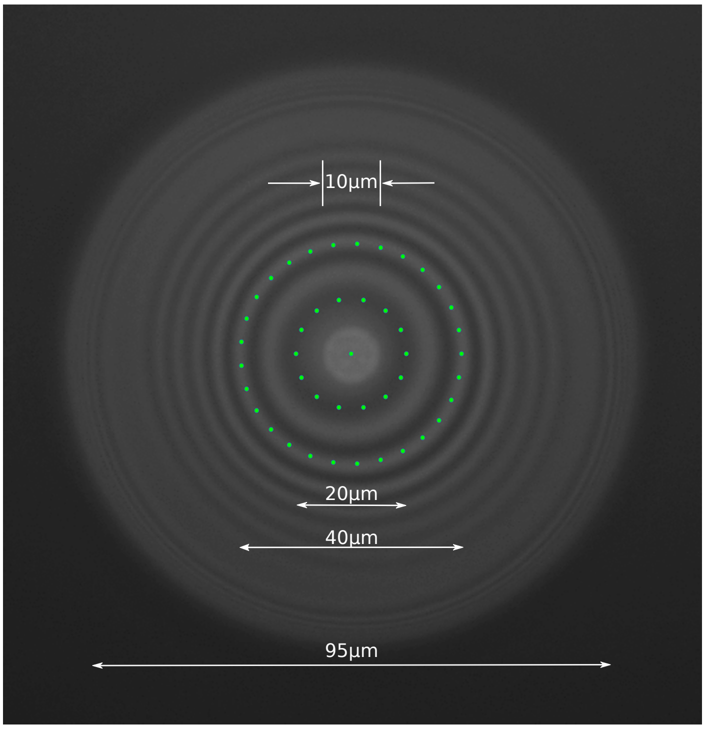

Figure 3.3.4: Interferometric picture of the machined structure on SM2000 fibre made with multishot technique. Total number of pulses: 46, pulse length $\tau = 16.5\,\mathrm{ms}$, power $(794 \pm 20)\,\mathrm{mW}$. The bright spot in the center is the fibre core and not part of the interferometric pattern.

The dimension of a structure on a fibre end facet is estimated by surface reconstruction and by fitting a Gaussian and spherical curve to the center of the structure. The cross sections for the horizontal and vertical direction for a SM2000 fibre are shown in figure 3.3.5. The large overlap of the Gaussian and spherical fit shows the successful structure shaping with the multishot technique. From the cross sectional fits, it can be claimed that the mirror structure has a diameter of at least 60 µm and shows a reasonably small ellipticity. From this, it can be concluded that the anticipated mirror diameters are reached for the above mentioned configuration.

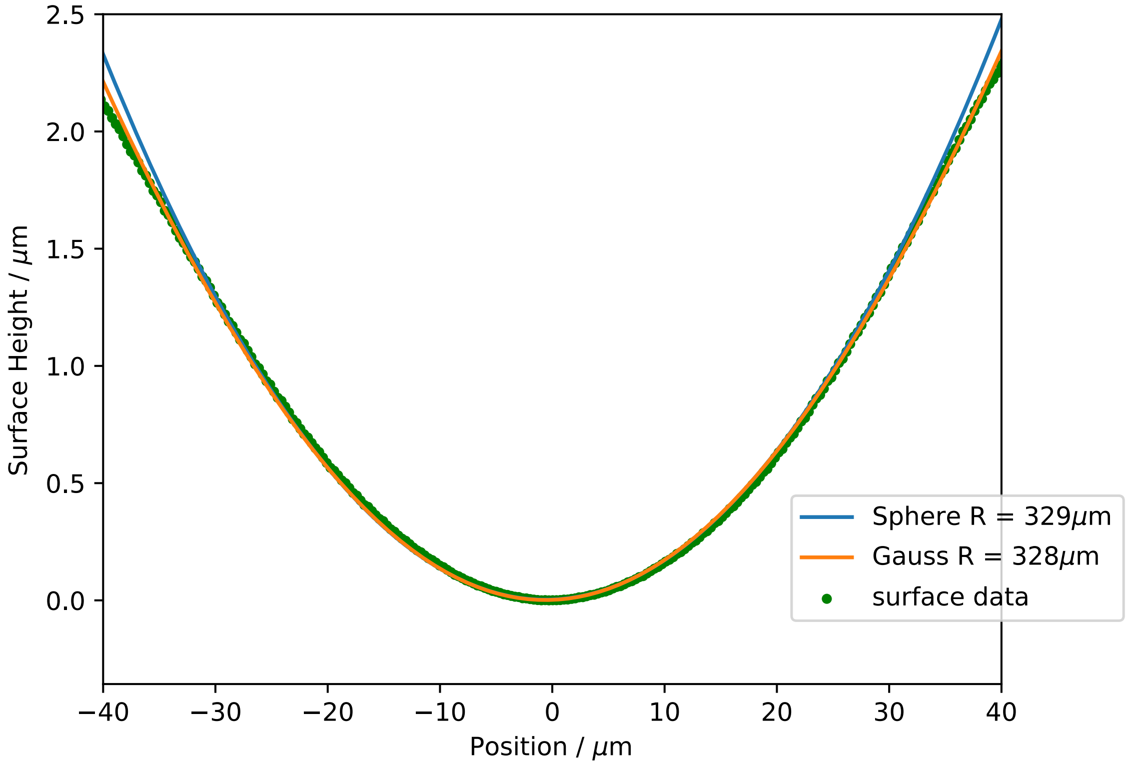

(a) Horizontal cross section.

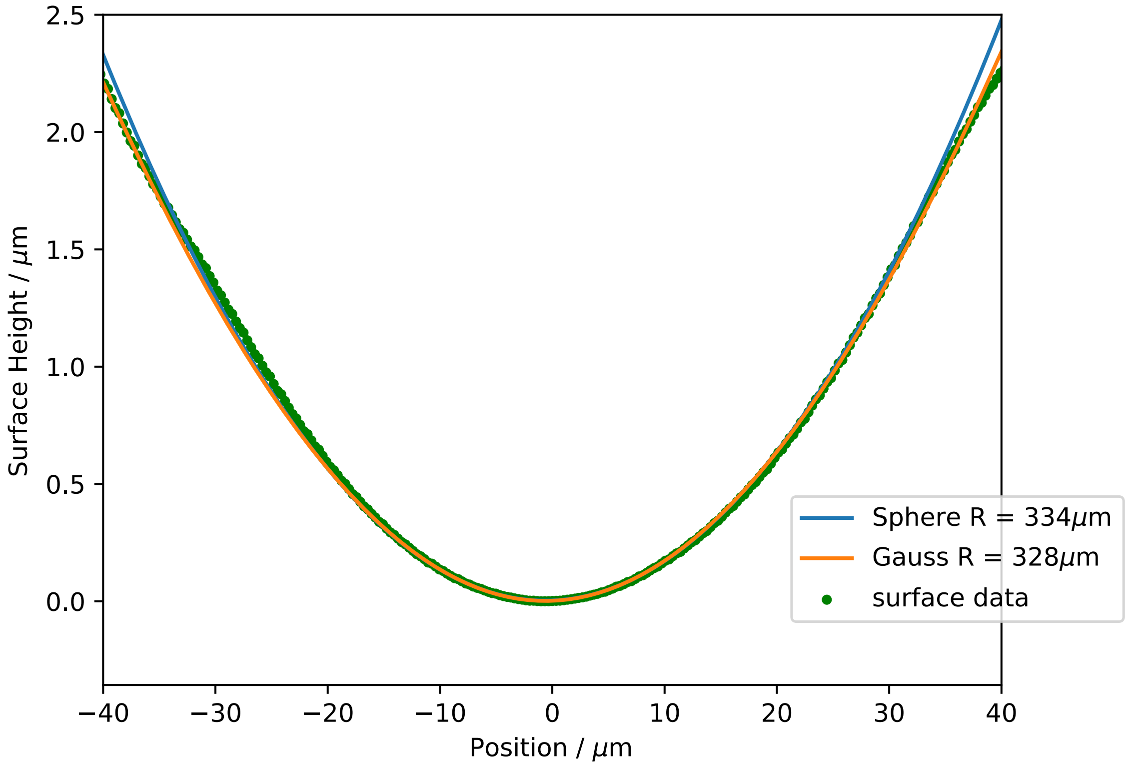

(b) Vertical cross section.

Figure 3.3.5: Cross section of reconstructed surface for a SM2000 fibre from interferometric data with multishot technique.

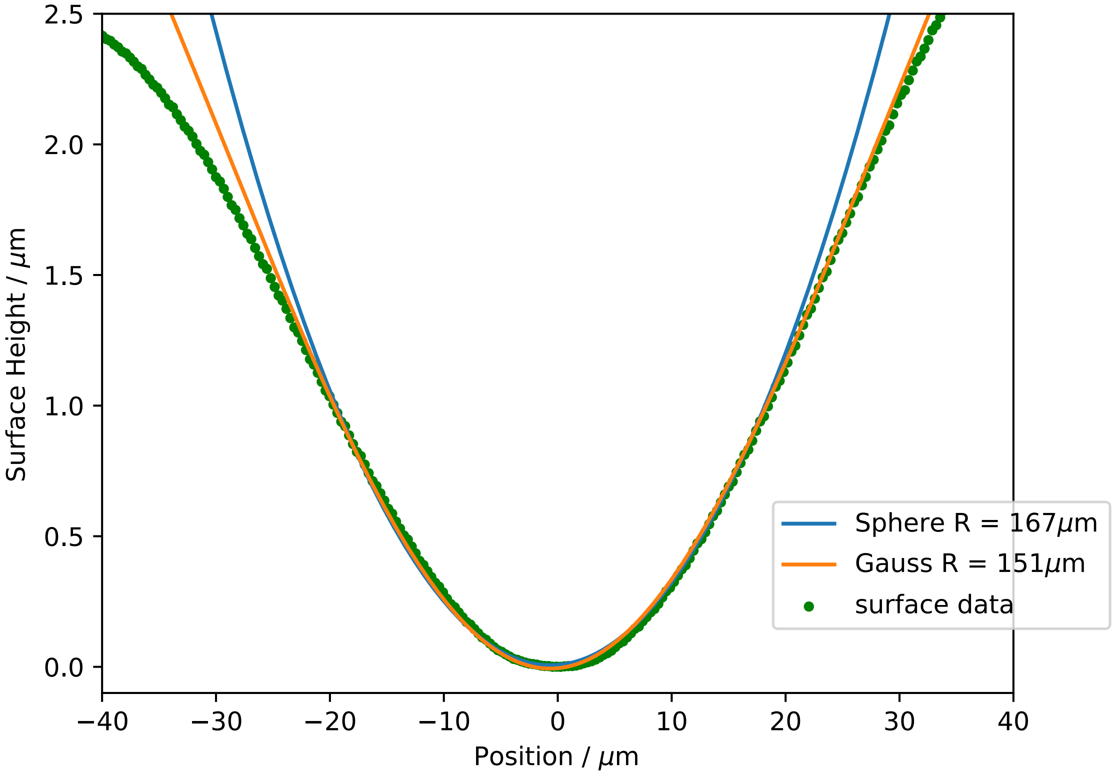

(a) Horizontal cross section.

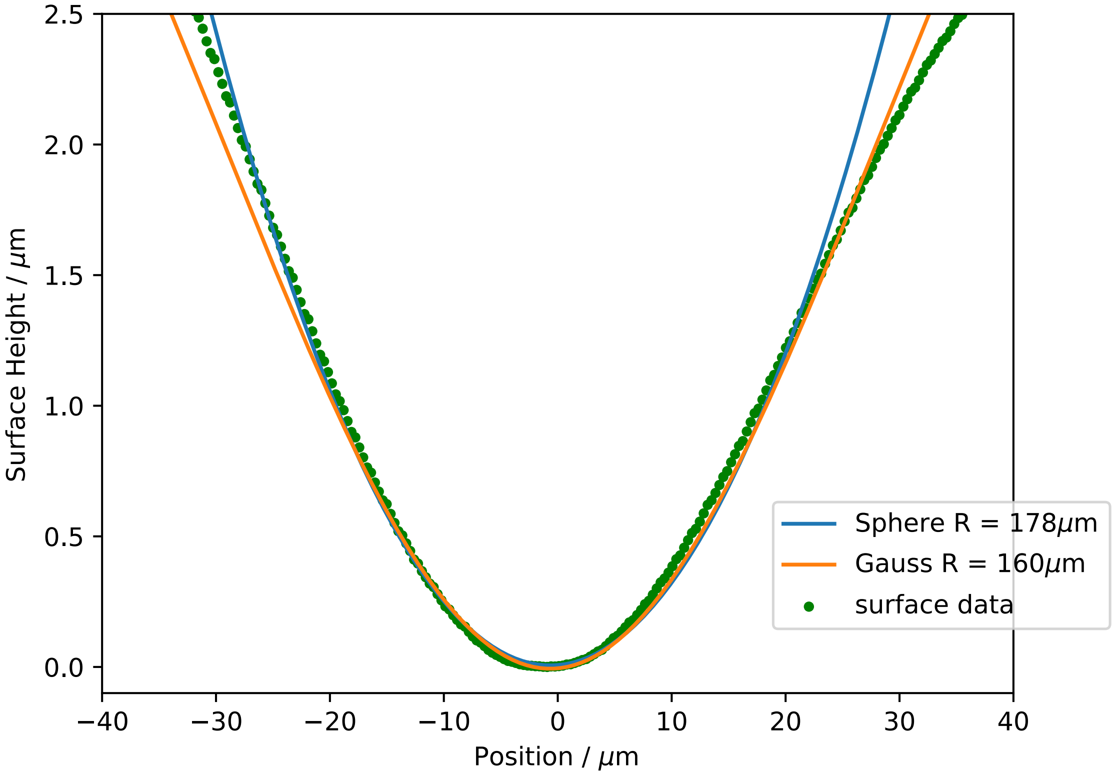

(b) Vertical cross section.

Figure 3.3.6: Cross section of reconstructed surface from interferometric data for a CU600 fibre using a single shot.

In comparison, the cross sections for a CU600 fibre shaped with one single shot are depicted in figure 3.3.6. It shows that applying one single shot restricts the Gaussian diameter in the center of the structure. One can see that the structure is much smaller for this technique but also yields satisfactory results. The mirror diameter is about 30 µm large which is sufficient for the light of 670 nm.

Finesse Measurement

For final confirmation of the fibre mirror's quality, the finesse for a plano-concave configuration is measured. One macroscopic mirror and one fibre mirror are placed such that the high-reflective surfaces face each other and form a resonator, see figure 3.3.7.

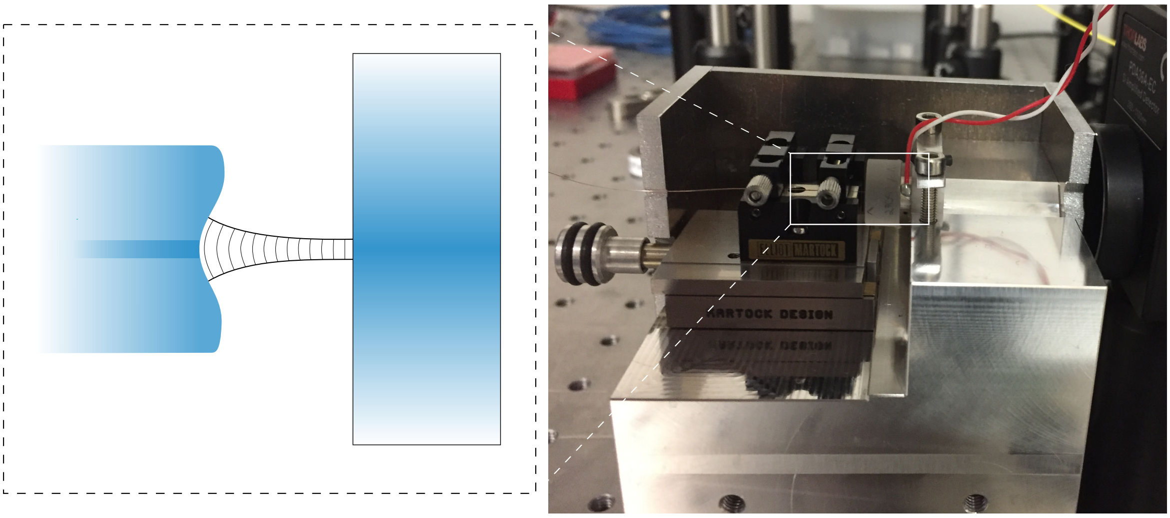

Figure 3.3.7: Stable mount for plano-concave cavity with one fibre mirror and a macroscopic mirror. Both surfaces have the same coating. The macroscopic mirror is attached to piezoelectric actuator to scan the cavity in length.

Light of 670 nm and 1988 nm is coupled into the corresponding fibre and the reflection signal of the cavity is recorded. For the finesse measurement of 670 nm light, side bands of 1.57 GHz are added with an electro-optical modulator to calibrate the timescale on the oscilloscope. Scanning the macroscopic mirror with a piezoelectric actuator, a reflection spectrum as depicted in figure 3.3.8 is visible with the photodiode. The manufacturer did measure the transmission spectrum for the created coating from the visible to infrared spectrum and provided the values on a graph. For a wavelength of 670 nm a transmission ratio of the coating can be read off as 1400 ppm. The finesse for 670 nm light is measured to be $\mathcal{F} = 1200 \pm 400$ which is of the same order as expected value of $\mathcal{F} \approx 2200$ for such a coating. The discrepancy of a factor of two should be compensated by further angle alignment.

At this point, the measurement of the finesse for 1988 nm could be roughly estimated from the ratio of the free spectral range over the peak width. A finesse of $\mathcal{F} = 7200 \pm 2400$ can be calculated although the measurement is subject to huge fluctuations. This values should only be treated as a preliminary result investigations are ongoing for further characterisation of the mirror surface. Thus, the obtained cavity is already a success especially since not the best fibres available have been used for

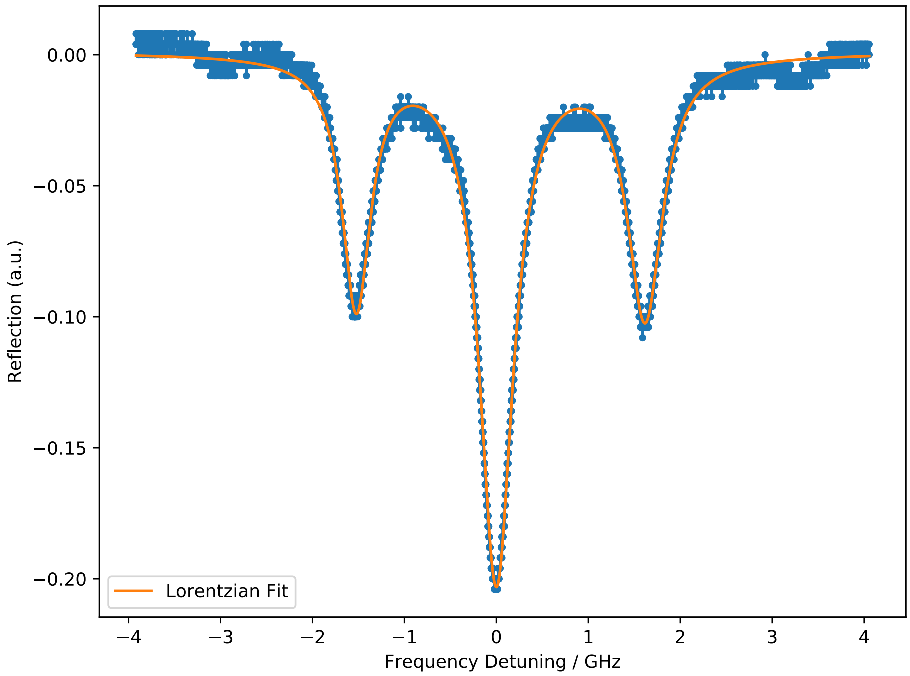

Figure 3.3.8: Reflection signal for the finesse measurement of a plano-concave fibre cavity for 670 nm light. Calculated values for the finesse $\mathcal{F} = 1379$ and FWHM $= 447\,\mathrm{MHz}$.

testing in order to leave the better ones for future experiments. The coating of the fibres and the substrates for a wavelength of 1988 nm is specified as $(160 \pm 50)\,\mathrm{ppm}$ which yields a calculated finesse of $\mathcal{F} \approx 20\,000 \pm 5000$.

Consequently, the measured finesse values approve the satisfactory functioning of the machining setup and demonstrates the ability of producing high quality fibre mirrors for high finesse resonators with this new-built setup. Further analysis is required in order to compare the fitted size of the reconstructed interferometer surface to the finesse measurement for different cavity lengths.

CHAPTER 4

Towards Integrated Electrodes on Fibre Mirrors

For studying atom-photon interactions and investigating the possibilities of constructing efficient optical interfaces, atoms are trapped inside optical resonators where they can be precisely manipulated. One way of positioning the charged atoms at a specific position is to use oscillating electric fields. Needle Paul traps, for instance, create a metastable saddle point in the trap center and offer large optical access to the ion due to their small sizes. However, motional heating limits the stability and the coherence time of the ion in the trap and the usability in quantum networks. For the construction of a reliable quantum network however, the two mentioned properties are relevant for the storage of a quantum bit and the information exchange. It is therefore essential to investigate and solve the limitations of the system. This chapter introduces the idea of integrating electrodes on fibre mirrors which could lead to further miniaturisation of ion traps and describes a promising way for overcoming the creation of uncontrolled static electric fields.

4.1 Paul Traps

The mass spectrometer invented by Wolfgang Paul in the 1950s [32] is the two-dimensional aforegoing version of the ion traps nowadays. Long time it was thought that charged particles cannot be confined in an electric potential, since Earnshaw's theorem [33] prohibits trapping with static fields, nevertheless it is possible to confine electrically charged particles in oscillating electric multipole fields. This is possible with an electric quadrupole field configuration of rotational symmetry which satisfies [34]

$$\Phi = \frac{\Phi_0(r^2 - 2z^2)}{r_0^2 + 2z_0^2} \quad \text{with} \quad r^2 = x^2 + y^2 \tag{4.1.1}$$

creating a potential with a metastable saddle point in the trap center. A superposition of a static DC voltage U and an alternating AC voltage V with frequency ω

$$\Phi_0 = U_{\text{dc}} + V_{\text{ac}} \cos(\omega t). \tag{4.1.2}$$

This leads to the equations of motions in r and z direction of the charged particle in the trap center

$$\ddot{x} + \frac{e}{mr_0^2}(U_{\mathrm{dc}} + V_{\mathrm{ac}}\cos(\omega t))x = 0 \tag{4.1.3}$$

$$\ddot{z} - \frac{e}{mr_0^2}(U_{\mathrm{dc}} + V_{\mathrm{ac}}\cos(\omega t))z = 0. \tag{4.1.4}$$

This periodic movement around the particles stability point can be rewritten in dimensionless parameters

$$\frac{\mathrm{d}^2 x}{\mathrm{d}^2\tau} + (a + 2q\cos(2\tau))x = 0 \tag{4.1.5}$$

$$\frac{\mathrm{d}^2 z}{\mathrm{d}^2\tau} - (a + 2q\cos(2\tau))z = 0 \tag{4.1.6}$$

where

$$a = \frac{4eU_{\mathrm{dc}}}{mr_0^2\omega^2}, \quad q = \frac{2eV_{\mathrm{ac}}}{mr_0^2\omega^2}, \quad \tau = \frac{\omega t}{2}. \tag{4.1.7}$$

The dimensionless parameters a and q express the ratio between the electric potential of the electrodes and the harmonic oscillator potential of the trap. The so-called Mathieu equations have stable and unstable solutions. In the first case, the particle executes an oscillation with limited amplitude whereas the latter executes an oscillation with growing amplitude which pushes the ion far outside the stability point and consequently prohibits the storage of the particle inside the trap. A stability diagram for a two-dimensional quadrupole field shows areas of stable and unstable solutions but only certain regions are of experimental interest. For experiments, the interesting region applies to $|a|, |q| \ll 1$ which means that the harmonic trap potential is much larger than the electric potential. The analytic first-order solution of the motion is [35]

$$u_i(t) \propto \underbrace{\cos(\Omega_i t + \phi_i)}_{\text{secular motion}} \underbrace{\left[1 + \frac{q_i}{2}\cos(\omega t)\right]}_{\text{micromotion}}, \quad u_i = x, y, z \tag{4.1.8}$$

which is a superposition of two oscillations with different frequencies. The frequencies depend on the voltage amplitudes of the static potential and the oscillating potential applied to the electrodes. The phase ϕ_i is determined by the initial position and the velocity of the ion. The oscillation of frequency ω is called *micromotion* and is solely driven by the alternating fields. The fast oscillation is the intrinsic reason of trapping and does not contribute to the kinetic energy of the ion. The *secular motion* denotes the harmonic oscillation with frequency Ω_i

$$\Omega_i \approx \frac{\omega}{2}\left(a_i + \frac{q_i}{2}\right). \tag{4.1.9}$$

which depends on the field amplitudes U_{dc} and V_{ac} and on the oscillating field frequency.

As soon as a ion is trapped, the kinetic energy of the ion can be further reduced via an optical cooling transition of resonant absorption and isotropic emission cycles. This allows to cool the ion to near the ground state of motion, i.e. to a thermal state with low vibrational quanta [36]. If the ion is also subject to a uniform static electric field, the equation of motion becomes

$$\ddot{u}_i + (a_i + q_i\cos(2\tau))\,u_i = \frac{eE_{\mathrm{dc}}}{m}u_i. \tag{4.1.10}$$

The ion is displaced from the trap centre and at the displaced average position, the AC electric field causes an *excess micromotion* which cannot be reduced by any cooling processes. As a consequence, external static electric fields disturb the motion of the ion in the trap, reduce its stability and shorten its coherence time which is essential for quantum computation.

4.2 Motivation

Static electric fields do influence the motion and the stability of an ion in a Paul trap [36]. These fields displace the ion from the trap center and the induced *excess micromotion* leads to the broadening of spectral lines of the ion due to the assotiated Doppler shift [35]. This motion reduces the lifetime of the ion in the trap [37] which is problematic for the long time storage of a quantum state. The creation of stray charges, more precisely randomly orientated dipoles, are recognized of being the source for motional heating of ions [38]. The creation of such dipoles should therefore be avoided which especially causes a problem when working with ultraviolet light. This is, the photoelectric effect is enhanced under the exposure of ultraviolet light [39] and light of small intensity easily releases dipoles from the trap electrodes. This causes a problem since the employed ions have strong optical dipole transitions in the ultraviolet spectrum and require an optical interface at the corresponding wavelengths. The stray charges created by the light field attach to various surfaces in the trap and load the entire surrounding. If a surface is an isolator, charges cannot discard, stick to their places and wreck all advantages of a needle Paul trap with a fibre cavity.
The dielectric layers of the high-reflectance coating on the fibre mirrors forming the optical interface are isolators and attract the released stray charges in the trap [40]. Attached to these surfaces, charges heavily influence the trap potential due to their location in the vicinity of the trap centre. By the employment of fibre cavities which have small sizes, the dielectric surface area is highly reduced which is a great advantage compared to former macroscopic interface implementations. In recent experiments, stray fields are shielded with grounded tubes around the fibres and nullified by applying a well-defined voltage to eight electrodes installed around the trap. The inserted tubes modify the desired trap potential and finding the compensating voltage for the compensation electrodes is however challenging.

It would therefore be advantageous to prevent stray charges from adhering to any dielectric surfaces and to be able to remove attached dipoles. For this reason, the idea of applying a conductive gold layer to the fibre mirrors has been developed. The applied gold coating pursues two aims. Firstly, the dielectric area which strongly attracts dipole charges is further reduced. And secondly, a well defined static potential can be applied to the coated areas which in future might replace the necessity of implementing external macroscopic electrodes. This is why there is the attempt to apply a continuous gold layer which functions as a ground potential and as separated electrodes. To achieve this, a couple of machining steps are necessary which might damage the mirror surfaces of the fibre cavity and could decrease the efficiency of the optical interface. The reflectivity of the mirrors, which is easily deteriorated by any particles on the surface, is essential for the construction of an efficient optical interface. The gold layer can therefore not be extended over the entire surface of the fibre but only to the boundaries of the fibre mirror which are not required for the reflection of the resonator mode. The mirror area which should not be coated with any additional layers should measure at least three times the resonator's mode diameter on the mirror surface in order to achieve clipping losses below 1 ppm, see equation 2.1.10. Hence, the electrode extension depends on the application parameters and should be adjusted accordingly. As optics are much better controlled in the infrared than in the ultraviolet spectrum, the first attempts for gold coating are all applied to optics that have high-reflectance coatings for a wavelength of 780 nm.

4.3 Realisation

The idea behind structuring the fibre mirrors is fairly easy. It requires a stencil which is attached to the fibre surface prior to gold coating and removed afterwards. The creation of three dimensional objects of the size down to 500 µm is possible with the precise 3D printer NanoScribe[1]. These objects are fabricated in cooperation with the group of Prof. Stefan Linden at the *Physikalisches Institut der Universität Bonn*. A two-photon polymerisation process in photosensitive materials on the scale of the focal spot size of the employed laser beam enables the creation of arbitrarily shaped structures on any surfaces. For increasing working efficiency, a fibre holder which holds up to 7 fibres has been developed. In contrast to the fibre holder employed for fibre machining, see chapter 3, the three-point bearing is made of a commercial glass v-groove and a spring on top of it, see figure 4.3.1a.

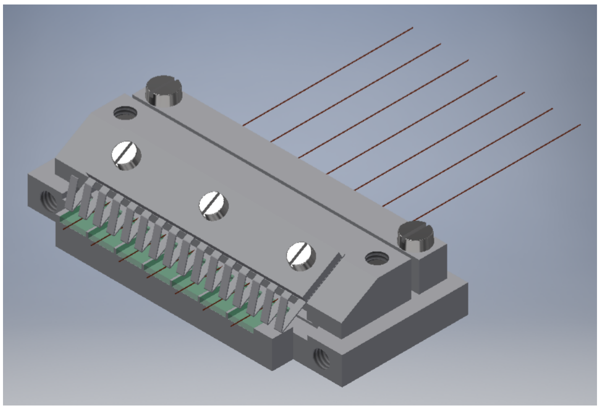

(a) Model of fibre holder for the NanoScribe. The glass v-groves are coloured in green, the fibres in orange.

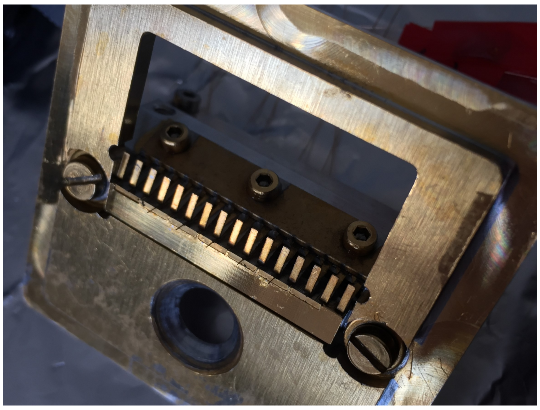

(b) Picture of the fibre holder with 5 fibres after the application of a gold coating.

Figure 4.3.1: Pictures of the fibre holder fitting in the NanoScribe for the creation of 3D structures.

The different machining steps needed for electrode structuring are depicted in figure 4.3.2. The fibre is put into the NanoScribe to write the protection mask on the desired regions. A viscous photosensitive material which is applied to the fibre tips

[1] `www.nanoscribe.de`

transforms into a rigid polymer at the spots which are illuminated by the laser beam focus. The concentricity of the written structure is guaranteed by aligning the visible fibre core (see figure 4.3.2a) with the centre of the NanoScribe structure. The central spherical part of the fibre mirror is covered by the stencil as well as by a spacing for the electrodes, see figure 4.3.2b. The entire structure is not directly attached to the mirror surface but stands on some feet, which shall allow for an easier removal after coating. To make sure that these feet stick to the glass surface, the polymerising laser beam is raised transversely from below the surface to above. Soaking the fibre ends into propylene glycol methyl ether acetate (PGMEA) dissolves the remaining viscous photoresist. After thorough cleaning with 99.99 % isopropyl alcohol, only the rigid mask remains on the fibre tip. The entire fibre holder is put into a coating chamber where a chromium layer of 5 µm and gold layer of 40 µm are evaporated onto the fibre mirrors. The chromium layer is coated below the gold layer for better adhesion properties. Afterwards, the NanoScribe structure is mechanically removed in a ultrasonic bath with ultrapure acetone. Eventually, the fibre end facets shall resemble figure 4.3.2c where the central part of the fibre is a perfectly reflecting dielectric surface while the outer part is split into four individual electrodes. The machining of the surface in the NanoScribe and the gold coating is entirely done by Alexander Fassbender. All works related to fibre preparation, to holder designs for machining and coating is part of this thesis.

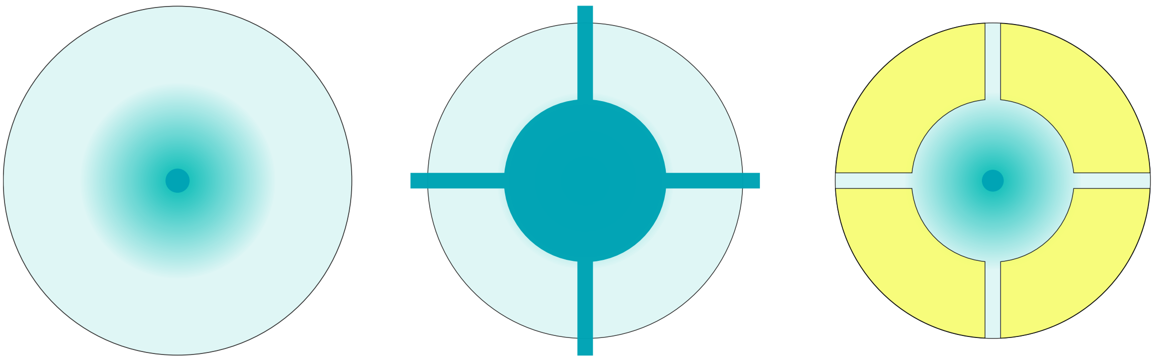

(a) Fibre with spherical central part and high-reflectance coating.

(b) Fibre mirror with NanoScribe structure.

(c) Fibre mirror with electrode structure, central part unmachined.

Figure 4.3.2: Machining steps for the creation of gold electrodes on fibre mirrors.

Prior to writing rigid structures onto fibre ends, for testing reasons, a fibre end facet was dipped into the viscous photosensitive material, cleaned with PGMEA and afterwards put in a ultrasonic bath. Finesse measurements have shown higher finesse values after applying these cleaning steps than before. This suggests that this machining part does not negatively effect the cleanness of the mirrors, and also removes dirt which was accidentally deposited on the mirror surface. Figure 4.3.3 shows the very first attempt of going through all machining steps without breaking the fibre end facet. The shown fibre is a CU600 fibre from IVG which has a flat cleaved surface without any coating. The creation of 3D structures on top of the fibre mirrors is very subtle. It is a extensive process to find the interface of the fibre surface with the NanoScribe since this machine is originally meant to print structures on flat substrates.

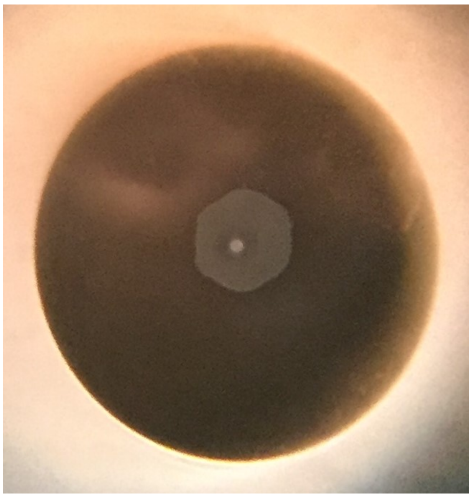

Figure 4.3.3: View of a fibre end facet through a light microscope. First try of a gold coated fibre facet without electrode structuring, the central part is unmachined.

So far there are no complete fibre electrodes which can be quantitatively explored. The writing of NanoScribe structures is learned on CU600 fibres from IVG which are only cleaved and do not have any mirror surface since the process needs to be perfected. In the first attempts, only one fibre out of five got through the entire machining process without breaking and real fibre mirrors are too precious to be wasted for development. The successful realization on a glass substrate is shown in figure 4.3.4.

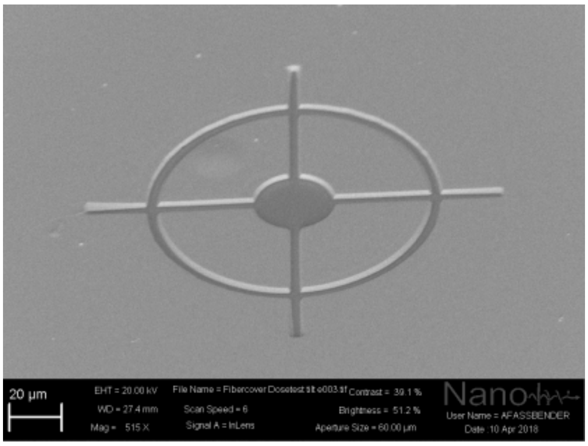

Figure 4.3.4: Picture of glass substrate were the desired NanoScribe structure has been attached to prior to gold coating. The pictures has been taken with a scanning electron microscope (SEM). Picture kindly provided by Alexander Fassbender.

The successful attachment of the protection mask onto a high-reflective macroscopic mirror substrate has also been demonstrated. This substrate has the same outermost coating layer as the fibre mirror and confirms that writing on high reflective surfaces works with the NanoScribe. This could have been a problem as one needs to find to the focus of the red laser beam which polymerises the photoresist and strong reflections might have prohibit this. Hopefully soon, the machining steps are done onto spherical surfaces and finally onto real fibre mirrors.

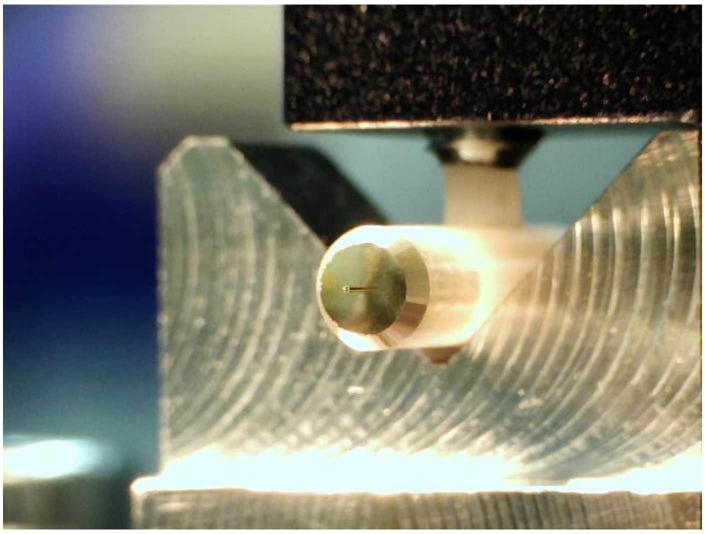

Figure 4.3.5: Golden fibre surface inserted into a gold coated fibre ferrule.

For practical applications, a way of connecting the individual electrodes needs to be developed. At first, there was the idea of connecting the surface layers to a macroscopic conductive object using wire bonding. Wire bonding is usually used to connect integrated electronic circuits by attaching a very thin gold wire with ultrasonic energy to the corresponding components. If connected to a macroscopic object, it could be easily connected to a macroscopic wire using soldering. Therefore, cleaved fibre surfaces and the end surface of fibre ferrules were coated with gold and the fibre inserted into the ferrule, see figure 4.3.5. In this configuration, it was tried to connect the fibre surface to the ferrule with thin gold wires, see figure 4.3.6. Unfortunately, it was found that the applied gold layer is far too thin for wire bonding since the gold layer does not adhere sufficiently to the glas and ceramic surface to resist the pulling of the wire. By default, gold layers of 1 µm are used to stand the wire bonding process. Evaporating so much gold on the fibre tips is not a solution as it is far too expensive and consequently, this idea was dismissed. Alternatively, one could think of using another conductive material to create the electrodes which is less expensive. Additionally, there also arises a problem because the bonds have a certain height. Above the fibre surface, they disturb the trapping potential of the trap and of the electrode fields if some voltage is applied. As the trap is only 200 µm long, the height of the bonds must be very limited, even for grounding purposes. This is why this technique might only be suitable for ground connections but not for electrode connections.

The entire project is still in its infancy and requires further testing of the coating layers. So far, some realisation on glass substrates and uncoated fibre end facets already showed promising results. Still, there are a few things that have to be confirmed as soon as there are complete fibre electrodes available. The electric isolation between the individual coating areas has to be demonstrated to ensure the proper functioning of the individual electrodes. This can only be done on fibre mirrors with curved surfaces as the carbon layer on the outside cladding of the copper coated fibres connects all electrodes together. In the vicinity of a fibre mirror surface the carbon is removed by the CO_2 laser pulse sequence of infrared light during ablation processes. Also the finesse needs to be measured with attached electrodes to confirm that the dielectric mirror surfaces have neither been negatively affected by the coating layers nor damaged by any previous machining step. If the finesse before and after electrode structuring does not show any degradation, the effort of machining electrodes on these small scales can be quantified as successful and useful.

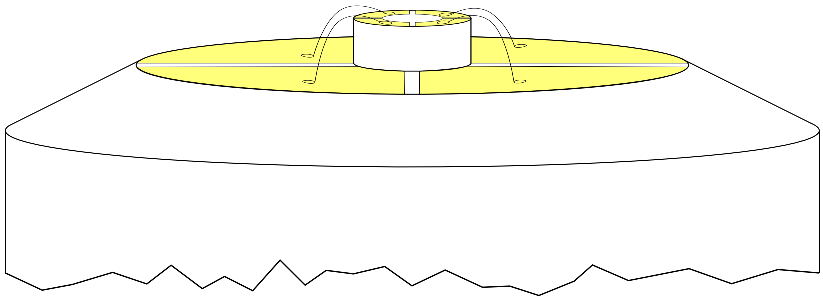

Figure 4.3.6: Sketch of wire bonding the fibre electrodes to the ferrule.

CHAPTER 5

Conclusion and Outlook

Conclusion

Fibre mirrors which allow for the construction of high finesse fibre cavities have been fabricated in the facilities of the *Institut für Angewandte Physik der Universität Bonn* for the first time. The rebuilt setup and the adoption of the graphical user interface for the machining process can now be used to create spherical structures on fibre end facets with two different machining techniques. The implementation of the AOM has shown the desired improvement in the reproducibility of surface shapes. The interferometric analysis confirms the achievement of the desired mirror geometries which have spherical central parts extending up to a diameter of 60 µm and inducing clipping losses of $\mathcal{L} \leq 1\,\mathrm{ppm}$. It has been shown that the produced fibre mirrors for the wavelength of 1988 µm yield a cavity finesse of $\mathcal{F} = 7200 \pm 2400$ and for the wavelength of 670 nm $\mathcal{F} = 1200 \pm 400$. For all future fibre shaping, a total number of 24 fibre holders adapted to the current setup are at the disposal of the two collaborating research groups. The successful application of a conductive gold layer on a fibre end facet has been demonstrated and encourages the development of ion traps as quantum nodes. All in all, the work during this thesis contributes technical knowledge to the challenges in the field of quantum networks.

Outlook

The finesse of a cavity built from the produced fibre mirrors needs more investigations in order to correlate the finesse measurements to the interferometric data of the surfaces. The finesse for cavities at 1988 µm should be measured using an EOM for different cavity lengths. There also is some room for improvements in the machining setup. As a next step, the power stabilisation has to get to work by replacing the pick-off plate. If this is done, it would be useful to calibrate the system so that the user only needs to choose certain geometry parameters and does not have to select the machining technique nor the pulse length or the power of the pulse. Additional to these steps, it would be useful to identify the element which causes thermal drifts of the laser beam and makes the fibre structuring unprecise. Also, with the current coupling lens, one risks to burn the capillary entry with high powers and consequently the spot size at the capillary entry should slightly be reduced.

APPENDIX A

Appendix

A.1 General Notes and Remarks

- Do not use the pick-off plate **WW71050-E3** from Thorlabs for power stabilisation. This plate seems to be polarisation sensitive though it is not specified by the supplier. A 50:50 beam splitter might be more convenient. Additionally a brewster plate has been ordered to clean the polarisation and improve power stabilisation.

- The coupling lens of $f = 500\,\mathrm{mm}$ is slightly too large for coupling into the hollow silica waveguide and prohibiting burning any edges. The mode waist diameter should measure 70 % of the waveguide diameter according to the manufacturer. In this setup, the tip of the capillary slightly turns dark if high power $\geq 1\,\mathrm{W}$ is coupled for times $\geq 2\,\mathrm{s}$ through the capillary. Especially if even more power is required for shooting, the lens should be replaced by another lens with shorter focal length. There are also proper fibre couplers commercially available which might solve this problem more easily.

- There is a element that is highly affected by thermal lensing. This effect is seen for light behind the pick-off plate and power that exceeds 1 W. In this case, the beam centre shifts in horizontal direction and prohibits proper power measurement since it does not hit the detection area over the entire measurement time.

- The coherent power meter reflects almost 5 % of the incident power. This reflection is not diffuse and needs to be blocked during measurements, especially with high power.

- When testing pulses on glass substrates, take care what material you use. There are some glass substrates which do not get Gaussian deformation, but a Gaussian deformation with a blob in the centre. If this happens, change the glass material! Achieving good spherical structures on glass plates doesn't mean they are creatable on fibre end facets. Glass substrates and fibre tips behave quite differently when exposed to infrared radiation.

A.2 Gaussian Beams

A beam is called a Gaussian beam when its radial intensity distribution is radial symmetric and can be written at any point of propagation z as [11]

$$I(r) = \frac{2P}{\pi w(z)} \exp\left(-2\frac{r^2}{w(z)^2}\right) \tag{A.2.1}$$

where P is the total power of the light field, r the distance from the center of the beam and w(z) is the $1/e^2$ radius of the intensity distribution. Moreover, the electric field distribution carries important information about the phase and the wavefront curvature that evolve with propagation in space

$$E(r,z) = E_0\frac{w_0}{w(z)} \exp\left(-\frac{r^2}{w(z)^2}\right) \exp\left(i\left(kz - \arctan\left(\frac{z}{z_R}\right) + \frac{kr^2}{2R(z)}\right)\right). \tag{A.2.2}$$

w_0 denotes the minimum beam waist, k the wavenumber $k = {}^{2\pi}/_{\lambda}$, z is the spatial propagation variable, z_R the Rayleigh length and $R(z)$ the wavefront curvature. The waist of a Gauss beam increases over distance from the minimum waist position as

$$w(z) = \sqrt{w_0\left(1 + \left(\frac{z}{z_R}\right)^2\right)}. \tag{A.2.3}$$

where z_R the Rayleigh length is defined as

$$z_R = \frac{\pi w_0^2}{\lambda}. \tag{A.2.4}$$

It describes the distance over which the Gauss beam waist enlarges by a factor of $\sqrt{2} \approx 1.41$ and can in praxis be treated to not diverge significantly over this distance. This information is in praxis useful to estimate how precisely an optical element, e.g. a lens, has to be placed on the beam path.

The wavefront curvature evolves as

$$R(z) = z\left(1 + \left(\frac{z}{z_R}\right)^2\right) \tag{A.2.5}$$

this is the phase profile is flat only at $z = 0$ which denotes the minimum waist position or focus.

Bibliography

1. Kimble, H. J. The Quantum Internet. *Nature* **453,** 1023 –1030 (2008).
2. Loss, D. & DiVincenzo, D. P. Quantum computation with quantum dots. *Phys. Rev. A* **57,** 120–126 (1 1998).
3. Cirac, J. I. & Zoller, P. Quantum Computations with Cold Trapped Ions. *Phys. Rev. Lett.* **74,** 4091–4094 (20 1995).
4. Briegel, H.-J., Calarco, T., Jaksch, D., Cirac, J. I. & Zoller, P. Quantum computing with neutral atoms. *Journal of Modern Optics* **47,** 415–451 (2000).
5. Childress, L. & Hanson, R. Diamond NV centers for quantum computing and quantum networks. *MRS Bulletin* **38,** 134–138 (2013).
6. Shor, P. Polynomial-Time Algorithms for Prime Factorization and Discrete Logarithms on a Quantum Computer. *SIAM Journal on Computing* **26,** 1484–1509 (1997).
7. Ritter, S. *et al.* An elementary quantum network of single atoms in optical cavities. *Nature* **484.** doi:`10.1038/nature11023`. `http://dx.doi.org/10.1038/nature11023` (2012).
8. Meyer, H. M. *et al.* Direct Photonic Coupling of a Semiconductor Quantum Dot and a Trapped Ion. *Phys. Rev. Lett.* **114,** 123001 (12 2015).
9. Purcell, E. M., Torrey, H. C. & Pound, R. V. Resonance Absorption by Nuclear Magnetic Moments in a Solid. *Phys. Rev.* **69,** 37–38 (1-2 1946).
10. Gallego, J. *et al.* Strong Pucell effect on a neutral atom trapped in an open fiber cavity. `https://arxiv.org/abs/1804.08526` (2018).
11. Saleh, B. & Teich, M. *Fundamentals of Photonics* ISBN: 9780471358329 (Wiley, 2007).
12. W. Kogelnik, H & Li, T. Laser Beams and Resonators. **5,** 1550–67 (Oct. 1966).
13. Gallego, J. *et al.* High Finesse Fiber Fabry-Perot Cavities: Stabilization and Mode Matching Analysis. **122** (Aug. 2015).
14. Durak, K, Nguyen, C. H., Leong, V, Straupe, S & Kurtsiefer, C. Diffraction-limited Fabry–Perot cavity in the near concentric regime. *New Journal of Physics* **16,** 103002 (2014).
15. Takahashi, H. *et al.* Novel laser machining of optical fibers for long cavities with low birefringence. *Opt. Express* **22,** 31317–31328 (2014).

16. Bick, A. *et al.* The role of mode match in fiber cavities. *Review of Scientific Instruments* **87,** 013102 (2016).

17. Brandstätter, B. *et al.* Integrated fiber-mirror ion trap for strong ion-cavity coupling. *Review of Scientific Instruments* **84,** 123104 (2013).

18. Hunger, D *et al.* A fiber Fabry–Perot cavity with high finesse. *New Journal of Physics* **12,** 065038 (2010).

19. Gulati, G., Takahashi, H., Podoliak, N., Horak, P. & Keller, M. Fiber cavities with integrated mode matching optics. **7** (Mar. 2017).

20. Cummings, F. & T. Jaynes, E. Comparison of quantum and semiclassical radiation theories with application to the beam maser, 89–109 (Jan. 1963).

21. Meystre, P. & Sargent III, M. *Elements of Quantum Optics* (Springer, 2007).

22. Fox, M. *Quantum Optics* (Oxford University Press, 2006).

23. Steiner, M., Meyer, H. M., Deutsch, C., Reichel, J. & Köhl, M. Single Ion Coupled to an Optical Fiber Cavity. *Phys. Rev. Lett.* **110,** 043003 (4 Jan. 2013).

24. Monroe, C. *Ion Periodic Table* `http://iontrap.umd.edu/resources-2/periodic-table/`. Accessed: 20.09.2018.

25. Friis, N. *et al.* Observation of Entangled States of a Fully Controlled 20-Qubit System. *Phys. Rev. X* **8,** 021012 (2 2018).

26. Garcia, S. *Interfaces fibrees entre atome uniques et photons uniques* PhD thesis (2017). `https://tel.archives-ouvertes.fr/tel-01382230v2`.

27. Ott, K. *Towards a squeezing-enhanced atomic clock on a chip* PhD thesis (2017). `https://tel.archives-ouvertes.fr/tel-01452767`.

28. Uphoff, M., Brekenfeld, M., Rempe, G. & Ritter, S. Frequency splitting of polarization eigenmodes in microscopic Fabry–Perot cavities. *New Journal of Physics* **17,** 013053 (2015).

29. Uphoff, M. *Optical microcavities for quantum communication with single atoms* Dissertation (Technische Universität München, München, 2017).

30. Kubista, M. A New Fiber Mirror Production Setup. `http://quantum-technologies.iap.uni-bonn.de/en/group-members/224-michael-kubista.html` (2017).

31. Langerfeld, T. F., Meyer, H. M. & Köhl, M. Correlated-photon-pair emission from a cw-pumped Fabry-Perot microcavity. *Phys. Rev. A* **97,** 023822 (2 2018).

32. Paul, W. & Steinwedel, H. Ein Neues Massenspektrometer Ohne Magnetfeld. **8,** 448 (July 1953).

33. Earnshaw, S. On the nature of the molecular forces which regulate the constitution of the luminiferous ether. *Trans. Camb. Phil. Soc* **7,** 97–112 (1842).

34. Paul, W. Electromagnetic traps for charged and neutral particles. *Rev. Mod. Phys.* **62,** 531–540 (3 1990).

35. Berkeland, D. J., Miller, J. D., Bergquist, J. C., Itano, W. M. & Wineland, D. J. Minimization of ion micromotion in a Paul trap. *Journal of Applied Physics* **83,** 5025–5033 (1998).

36. Deslauriers, L. *et al.* Scaling and Suppression of Anomalous Heating in Ion Traps. *Phys. Rev. Lett.* **97,** 103007 (10 2006).
37. Ballance, T. G. *An ultraviolet fibre-cavity for strong ion-photon interaction* PhD thesis (Magdalene College, University of Cambridge, 2016).
38. Safavi-Naini, A., Rabl, P., Weck, P. F. & Sadeghpour, H. R. Microscopic model of electric-field-noise heating in ion traps. *Phys. Rev. A* **84,** 023412 (2 2011).
39. Hertz, H. Ueber einen Einfluss des ultravioletten Lichtes auf die electrische Entladung. *Annalen der Physik* **267,** 983–1000 (1887).
40. Harlander, M, Brownnutt, M, Hänsel, W & Blatt, R. Trapped-ion probing of light-induced charging effects on dielectrics. *New Journal of Physics* **12,** 093035 (2010).